RESEARCH ARTICLE

Effector-mediated plant lipoxygenase protein relocalisation triggers susceptibility

Indira Saado[1,2], Khong-Sam Chia[1,2,3], Ruben Betz[1,2], André Alcântara[1,4], Aladár Pettkó-Szandtner[5], Fernando Navarrete[1,6], John C. D'Auria[2], Michael V. Kolomiets[7], Michael Melzer[2], Ivo Feussner[8], Armin Djamei[1,2,9]

[1]Gregor Mendel Institute (GMI), Austrian Academy of Sciences (OEAW), Vienna BioCenter 7(VBC), Dr. Bohr-Gasse 3, 1030 Vienna, Austria

[2]Current address: Leibniz Institute of Plant Genetics and Crop Plant Research (IPK), OT Gatersleben, Corrensstraße 3, D-06466 Stadt Seeland, Germany.

[3]Current address: The John Innes Centre, Norwich Research Park, Norwich, NR4 7UH, United Kingdom

[4]Current address: Austrian Institute of Technology GmbH (AIT), Giefinggasse 4, 1210 Vienna, Austria

[5]Current address: Biological Research Centre, Hungarian Academy of Sciences Temesvari krt. 62, H-6726, Szeged, Hungary

[6]Current address: Centre for Research in Agricultural Genomics (CRAG), CSIC-IRTA-UAB-UB, Campus UAB, Bellaterra, Spain.

[7]Texas A&M University (TAMU), 496 Olsen Blvd, 77843-2132, College Station, Texas, United States

[8]University of Göttingen, Albrecht-von-Haller Institute for Plant Sciences and Goettingen Center for Molecular Biosciences (GZMB), Department of Plant Biochemistry, Justus-von-Liebig Weg 11, 37077, Göttingen, Germany

[9]Current address: Institut für Nutzpflanzenwissenschaften und Ressourcenschutz (INRES) der Universität Bonn, Pflanzenpathologie, Nussallee 9, D-53115 Bonn

Corresponding Author: adjamei@uni-bonn.de

Short title: Rip1 effector relocates Lox3 to suppress immunity

One sentence summary: Fungal PTI-inhibiting effector Rip1 relocalizes maize lipoxygenase 3 to the plant nucleus to suppress PAMP-triggered ROS-burst responses.

The author responsible for distribution of materials integral to the findings presented in this article in accordance with the policy described in the Instructions for Authors (www.plantcell.org) is: Armin Djamei (adjamei@uni-bonn.de)

ABSTRACT

The gall-inducing, biotrophic, maize-colonizing fungus *Ustilago maydis* secretes a complex effector blend in order to suppress defence and redirect host metabolism in its favor. Coevolution between the pathogen effectome and the host plant immune system shapes a multifaceted molecular network of interactions that remain phenotypically unrecognized and functionally elusive unless single players are depleted from the system. Here, we elucidate the ROS burst interfering protein 1 (Rip1) effector, which is involved in suppression of PAMP-triggered immunity suppression during biotrophy. We demonstrate its functional conservation in several monocot infecting smuts and identified a conserved, short C-terminal motif which is essential for Rip1-mediated PAMP-triggered ROS-burst suppression. We found the maize susceptibility factor lipoxygenase 3 (Zmlox3) to be directly bound by Rip1 and relocalised to the plant nucleus. Nuclear relocalisation of Zmlox3 leads to partial ROS-burst suppression. This function is independent of its enzymatic activity revealing a so far non-identified activity independent function of ZmLox3. Most importantly, whereas Zmlox3 maize mutants show increased resistance to *U. maydis* wildtype strains, rip1 deletion strains infecting Zmlox3 mutant overcome this effect. This could indicate that Rip1-triggered host resistance depends on ZmLox3 to be suppressed and that lox3 mutation-based maize resistance to *U. maydis* is dependent on the presence of functional Rip1. Together our results reveal, that the *U. maydis* effector Rip1 acts in several cellular compartments as PTI-suppressor and that targeting of ZmLox3 by Rip1 is responsible for the suppression of Rip1- dependent reduced susceptibility of maize to *U. maydis*.

Introduction

Plant colonisation by biotrophic pathogens requires sophisticated strategies for tissue invasion, defence suppression and metabolic manipulation to loot nutrients necessary for their growth and reproduction. The gall-inducing, biotrophic fungus *Ustilago maydis* secretes a multifaceted effectome during maize plant colonization to achieve the abovementioned tasks. Co-evolutionary forces on the effectome and the corresponding host immune system shape plant-pathogen interactions and are summarized in the famous ZigZag model, where pathogen recognition by host immune receptors and recognition suppression by new effectors lead to compatible or incompatible interactions over the evolutionary lifespan of this interaction (Jones and Dangl, 2006). Building on the Co-evolution process leading to effector triggered immunity (ETI) and effector triggered susceptbiity (ETS), the iceberg model addresses the point that only few nucleotide-binding domain leucine-rich repeat containing (NLR) - effector combinations are genetically visible as NLR/avirulence effector pairs. The vast majority stays in the interaction phenotypically silent due to ETS. This is supposed to be symbolized by the iceberg of which also only a minor part is visible above water level (Thordal-Christensen, 2020). Although the *Ustilago hordei* avr/R gene interactions have been described (Ali et al., 2014), avr-triggered R gene responses in the *U. maydis*/maize pathosystem have not yet been identified.

Most of the 1300 species among the smut fungi cause their disease symptoms in the floral organs, rather exceptionally, *U. maydis* is able to cause gall-formation on all aerial parts of its host plant *Zea mays* and its predecessor teosinte (Bauer et al., 2001). To date, *U. maydis* effector proteins were shown to act in various tissues and subcellular compartments targeting and modifying different molecules involved in plant immunity (Darino et al., 2021; Giraldo and Valent, 2013; Hemetsberger et al., 2012; Navarrete et al., 2021b). Generally, one differentiates between apoplastic effectors (Doehlemann et al., 2009; Fukada et al., 2021; Mueller et al., 2013) that are acting in the biotrophic interphase between the fungus and its host, and so called translocated effectors which act in the symplast (Darino et al., 2021; Djamei et al., 2011; Kämper et al., 2006; Lo Presti et al., 2015; Navarrete et al., 2021a; Redkar et al., 2015; Tanaka et al., 2014; Uhse and Djamei, 2018).

The plant immune system perceives attacks by two major types of receptors. Pattern recognition receptors (PRRs) recognize conserved non-self molecules (pathogen associated molecular pattern (PAMPs), or damage associated molecular patterns

(DAMPs) leading to pattern triggered immunity (PTI). Pathogen-specific effectors, or their activity, are perceived by NLR proteins leading to the strong effector-triggered immunity (ETI) responses (Boller and Felix, 2009; Yuan et al., 2021). The PAMPs/PRRs interaction induces intracellular signaling cascades that include a cytosolic Ca^{2+} burst (Jeworutzki et al., 2010; Nomura et al., 2012; Ranf et al., 2011), rapid extracellular ROS production (Chinchilla et al., 2007; Nühse et al., 2007) and involvement of other small molecules such as nitric oxide and lipids (Foissner et al., 2000; Okazaki and Saito, 2014; Raho et al., 2011). These signals trigger a dynamic transcriptional reprogramming, leading to metabolic adaptations in the plant cells which results in restricting pathogen colonization (Moore et al., 2011). ROS-accumulation is not restricted to PTI-triggered immunity but is also involved in the ultimate outcome in the ETI in form of the hypersensitive response that leads to cell death. The partial dependency of ETI on functional PTI has been recently underlined by genetic evidence placing the NADPH oxidase RBOHD as a central integrator of both signaling pathways (Yuan et al., 2021, Ngou et al., 2021a).

One example of how the downstream signaling after effector recognition occurs has been shown for the TIR-NBS-LRR NLR protein, Rps4, which needs to be translocated to the nucleus to trigger a hypersensitive response (Sohn et al., 2014). This activity depends on its interaction with EDS1, a lipase-like nucleo-cytoplasmic protein that interacts with another lipase-like protein, PAD4. Both of these lipase-like proteins are involved in downstream signaling induced by a number of NLRs. Although the N-terminal lipase domain of EDS1 and PAD4 is conserved, it has been shown that its activity is not needed for its function downstream of ETI (Dongus and Parker, 2021; Lapin et al., 2020; Wagner et al., 2013).

Plant oxylipins are metabolites that are involved in numerous plant physiological processes including plant defence (Genva et al., 2019; Wasternack and Feussner, 2018). Biosynthesis of oxylipins starts with the oxygenation of polyunsaturated fatty acids such as linolenic acid (18:3) yielding reactive hydroperoxides which are then substrates for either 9- or 13-lipoxygenases (LOX), α-dioxygenases (α-DOX), or monooxygenases. The resulting molecules represent a host of different oxygenated derivatives. Lipid hydroperoxides can also degrade into reactive α,β-unsaturated oxo compounds capable of crosslinking proteins and DNA (Gaschler and Stockwell, 2017). Immunolabelling of LOX-enzymes in plants indicates so far a cytoplasmic or plastid

localization (Demchenko et al., 2012)(Feussner et al., 1995). Maize 9-LOX accumulates in plastids, cytoplasm and tonoplasts (Tolley et al., 2018).

LOX-derived oxylipins play an important role in plant defence responses (Cacas et al., 2005; Christensen and Kolomiets, 2011; Estelle et al., 2020). For example, many 13-LOX–derived compounds, including jasmonic acid (JA), 12-oxophytodienoic acid (OPDA), and 13-hydroxyoctadecatrienoic acid (13-HOT), regulate plant defence responses. Besides the 13-LOX pathway, the 9-LOX pathway was shown to activate defence responses against *Pseudomonas spp* in *Arabidopsis thaliana* (Vicente et al., 2012) or *Fusarium verticillioides* in maize (Christensen et al., 2014). Furthermore, genetic and biochemical evidence supports Zmlox3 belonging to the group of 9-LOX in *Z. mays.* It negatively modulates the PAMP-triggered extracellular ROS-burst. For several fungal pathogens including *U. maydis,* Zmlox3 was shown to be a susceptibility factor, disruption of which results in increased resistance (Gao et al., 2007; Pathi et al., 2020).

In this study, we functionally characterize the **R**OS-burst-**i**nterfering effector **p**rotein Rip1 (UMAG_04039) of *U. maydis* and provide evidence that this effector suppresses PAMP-triggered ROS in various subcellular compartments. Importantly, we provide biochemical and genetic evidence that Rip1 targets Zmlox3 to suppress PTI and Rip1-mediated reduction of susceptibility of maize to *U. maydis*. On the mechanistic side, we demonstrate that Rip1 relocates Zmlox3 to the nucleus and that nuclear Zmlox3 independent of its enzymatic activity leads to a reduced PAMP-triggered ROS-burst responsiveness in plants, explaining partially the ROS-burst suppressive activities of Rip1. We demonstrate functional conservation for various Rip1 orthologs and identify a short, conserved, C-terminal motif that is essential for its ROS-burst suppressive activity *in planta.*

Results

Rip1 is a small secreted fungal protein with ROS inhibiting activity in plants

Rip1 is a putative *U. maydis* effector without known functional domains or motifs, except for a predicted canonical signal peptide of the first 26 amino acids (aa) at the very N-terminal part of the protein (SignalP 5.0) (Almagro Armenteros et al., 2019) (Supplementary Fig. 1A). In the genome of *U. maydis*, the *rip1* gene is located on chromosome 11, contains an intron (position 276-367) and encodes a 166 aa long

protein (Supplementary Fig. 1A). Unlike many other putative effector candidates in *U. maydis*, *rip1* is not positioned in a cluster of other, co-regulated secreted protein-encoding genes. Rip1 has orthologs in various smut species belonging to Ustilaginaceae (Schuster et al., 2018) including *Sporisorium reilianum* (Sr14946)*, Sporisorium scitamineum* (SPSC_05323)*, Ustilago hordei* (UHOR_13428)*, Ustilago bromivora* (UBRO_13428) and *Melanopsichium pennsylvanicum* (BN887_05943). Transcriptomic time course experiments on *U. maydis* infected maize show a significant upregulation of *rip1*, peaking four days post infection (Supplementary Fig. 1B) (Lanver et al., 2018). In order to test whether Rip1 is a secreted effector during fungal infection, we generated Rip1-mCherry fusions with or without signal peptide under the control of a strong biotrophy-induced promoter, Cmu1 (Djamei et al., 2011). The unambiguous localisation at the edges of fungal hyphae and fungal tip indicated a secretion of Rip1 by *U. maydis,* which was not observed for $Rip1_{27\text{-}166}$-mCherry lacking its signal peptide (Fig. 1A). By osmolyte-induced plasmolysis of infected maize leaf cells, free diffusion of full length Rip1-mCherry in the biotrophic interphase between the fungus and the maize cells could be shown (Supplementary Fig. 1C). Lastly, we verified the secretion of Rip1 in axenic culture. We took advantage of the AB33 strain, in which b-filamentous growth can be induced by changing the nitrogen source (Brachmann et al., 2001). The detection in western blot of P_{otef}::$Rip1_{1\text{-}166}$-3xHA in both fractions, pellet and supernatant, confirms, that the protein contains a functional signal peptide. In comparison, a non-secreted protein, actin, was used as a lysis control and was only detected in the pellet fraction (Fig. 1B).

Many pathogen-derived effectors target PTI defence signaling in plants and the PAMP-triggered ROS-burst response is one of the earliest responses in PAMP-signaling. Therefore, we tested if Rip1 shows PTI suppressive activity by measuring PAMP-induced ROS-accumulation *in planta*. Maize plants transiently expressing Rip1 lacking its endogenous signal peptide were used to retain accumulation in the native host system. For transient expression, a foxtail mosaic virus vector was employed for virus-mediated overexpression of a p19-p2A-$Rip1_{27\text{-}166}$-HA-p2A-mCherry construct, introduced into whole maize seedlings through biolistic bombardment (Bouton et al., 2018). The p2A ribosome skipping motifs (Kim et al., 2011) in the transformed construct avoids a large tag that might interfere with Rip1 activity, while still being able to monitor successful transformation and protein expression by fluorescence

microscopy. The p19 protein is a silencing suppressor that counteracts putatively induced transgene-silencing of the host. Successfully transformed maize leaves were observed after 7 days post bombardment by confocal microscopy and the integrity of the fused proteins was confirmed by immunoblotting (Supplementary Fig. 1D and Supplementary Fig. 1E). Afterwards, leaf discs of transformed leaf regions were excised, challenged with the PAMP flg22 and ROS accumulation was determined by a luminol-based assay, measuring chemiluminescence as a proxy for H_2O_2 production (Smith and Heese, 2014). Indeed, Rip1 expression led to a significant suppression of PAMP-triggered ROS accumulation compared to our control plants expressing p19-p2A-mCherry-p2A-GFP (Fig. 1C). To elucidate if the host-target of Rip1 is conserved between monocots and dicots, we chose the dicot plant *Nicotiana benthamiana*. For expression of Rip1 in *N. benthamiana*, leaves were infiltrated with *Agrobacterium tumefaciens* containing either P_{35S}::Rip1$_{27\text{-}166}$-p2A-mCherry constructs or P_{35S}::mCherry as control. Two days after infiltration, leaf discs were excised, and further used to measure flg22-triggered ROS burst activities. Rip1$_{27\text{-}166}$ expression led to a strong suppression of ROS accumulation in comparison to the control, indicating that Rip1 acts as a potent interspecies ROS burst suppressor (Supplementary Fig. 1F). To rule out that non-responsiveness of Rip1 expressing plants to the PAMP-treatment is based on local cell-death of the plant tissue, we used trypan blue tissue staining to document that no enhanced cell-death occurs upon Rip1 expression in *N. benthamiana* (Fernández-Bautista et al., 2016) (Supplementary Fig. 1G). To further assess the localisation of Rip1 within plant cells, using biolistic transformation in *Z. mays* or *A. tumefaciens* mediated transformation in *N. benthamiana*, Rip1$_{27\text{-}166}$-mCherry-myc expression constructs were delivered into the respective plant cells and Rip1$_{27\text{-}166}$--mCherry-myc localisation was observed through confocal microscopy. Rip1$_{27\text{-}166}$--mCherry-myc is localized to both nucleus and cytoplasm (Fig. 1D and Supplementary Fig. 1H). In order to see if the mCherry fusion protein of Rip1 shows ROS suppression activity and if a specific subcellular localization can be correlated to it, we conducted a mislocalisation assay followed by flg22-induced ROS-production measurements. Microscopic analysis verified the respective mislocalisations of differently tagged Rip1$_{27\text{-}166}$ versions in *N. benthamiana* and the integrity of the fused proteins was confirmed by western blot (Supplementary Fig. 1I and 1J). Strikingly, misdirection of Rip1 to different cellular compartments by fusing a N-terminal myristoylation signal (MYR) targeting it to the inside of the plasma membrane) or c-

terminal NLS (nuclear localisation signal), targeting Rip1 into the plant nucleus or c-terminal NES (nuclear export signal), targeting the effector from the nucleus to the plant cytoplasm), demonstrated highly significant ROS burst suppressive activities of Rip1 in all tested cellular (sub-) compartments (Fig. 1E). We further noticed that infiltrations of *A. tumefaciens* suspensions with an OD_{600} at 0.2 in *N. benthamiana* plants show an almost complete ROS burst suppression for all Rip1 generated constructs. Therefore, we additionally tried infiltrations with different OD adjustments to reduce overall effector expression in the plant as excessive amounts of Rip1 in the plant cell might already saturate the system and therefore no subcellular activity preference for Rip1 is detectable. Despite the agrobacterial load reduction to OD_{600} set at 0.05 we still observed a strong ROS-burst suppression in *N. benthamiana* triggered by flg22 (Supplementary Fig. 1K) and no subcellular preferences of Rip1 activity was obvious.

Using ipool-seq, we have previously demonstrated that Rip1 deletion has no significant impact on virulence in seedling infection assays under laboratory conditions (Uhse et al., 2018). In addition, to elucidate if SG200Δrip1 has an organ specific phenotype we performed tassel infection assay (Redkar and Doehlemann, 2016), which show no significant difference to the progenitor strain SG200 (Supplementary Fig. 1L). This result is not surprising considering the functional redundancy of symplastic PTI-inhibiting effectors, which have been identified so far in the *U. maydis* effectome (Darino et al., 2021; Navarrete et al., 2021b, 2021a).

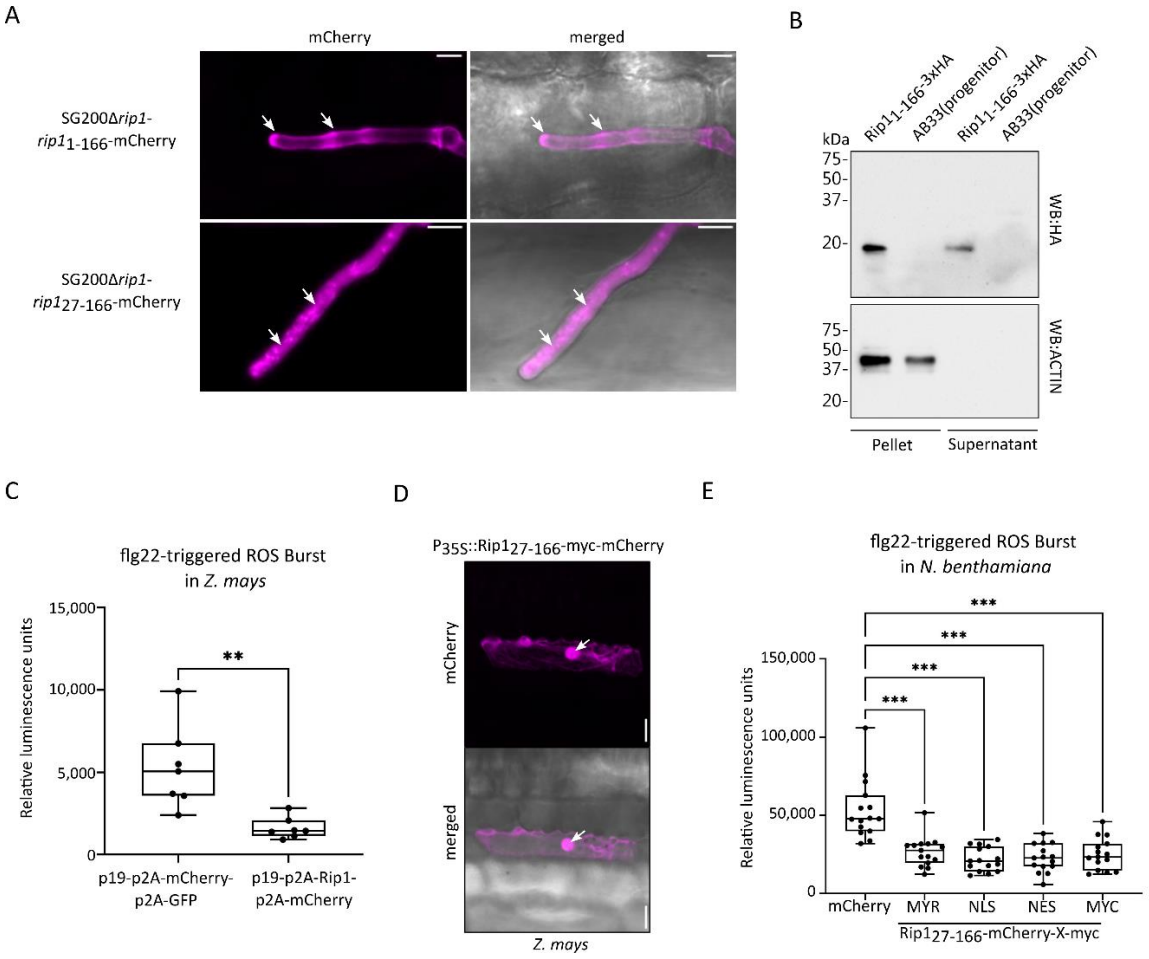

Figure 1: Rip1 is a fungal secreted protein which suppresses PAMP-triggered ROS burst in several subcellular compartments of a plant cell. A. Secretion of Rip1 in infected maize plants. Areas of cells from maize cv. B73 infected with *U. maydis* strains expressing mCherry fusions of Rip1 with (P_{Cmu1}::$Rip1_{1-166}$) or without signal peptide (P_{Cmu1}::$Rip1_{27-166}$) under the Cmu1 promoter are shown. Fluorescence was observed 5 days post infection. While secreted Rip1 strongly accumulates at the cell periphery of the hyphae and hyphal tip, localisation of Rip1 without signal peptide is evenly distributed within the hyphae, thereby forming aggregates (exemplarily indicated with white arrowheads). Scale bar = 5 µm. **B.** Secretion of Rip1 in axenic culture. $Rip1_{1-166}$-3xHA was expressed in the strain AB33 under the constitutive otef promoter. Total proteins were extracted from the pellet and secreted proteins were precipitated from the culture supernatant. The extracts were subjected to western blot with anti-HA or anti-Actin antibodies. $Rip1_{1-166}$-3xHA could be detected in both, pellet and supernatant whereas the non-secreted control, actin, was only detected in the pellet fraction. **C.** PAMP-triggered ROS burst assays in *Z. mays*. ROS accumulation in *Z. mays*, transiently overexpressing p19-p2A-$Rip1_{27-166}$-p2A-mCherry was monitored over 40 min after challenging with flg22. Plants expressing p19-p2A-mCherry-p2A-GFP were used as reference controls. Box plots indicate total accumulation of plant derived apoplastic ROS after PAMP-treatment based on detection of luminescent emissions. Displayed data show a pool of three biological replicates calculated for the total area under the curve; *Z. mays* n=7. Asterisks indicate statistically significant differences from the control (**p<0.01, Students t-test). **D**. Localisation of Rip1 (without signal peptide) in *Z. mays*. Transient expression of P_{35S}::$Rip1_{27-166}$-myc-mCherry via biolistic bombardment in maize plant leaves was observed through confocal

microscopy. Rip1 showed a nucleo-cytoplasmic localisation. Arrows exemplarily mark plant cell nuclei. Scale bar = 20 µm. **E.** Subcellular mis-localisation assays of Rip1 reveal its ROS burst suppression activity to be independent of the tested subcellular localisation. In *N. benthamiana* transiently expressed $Rip1_{27\text{-}166}$ fused to different subcellular localisation signals (MYR, NLS and NES) (x stands for either NLS or NES whereas MYR is fused to the N-terminal part of $Rip1_{27\text{-}166}$) shows ROS burst suppression activity in all subcellular compartments tested. Depicted data is a pool of three biological replicates; n=15. Asterisks indicate statistically significant differences from the control (*** $p<0.001$, one-way ANOVA followed by Tukey's test).

Functional analysis of Rip1 orthologs from other smut fungi leads to identification of a unique ROS-burst suppressive motif

Homology searches of the Rip1 protein sequence revealed several orthologs in other smut fungi (Supplementary Fig. 2A). To address the question whether Rip1 orthologs have similar functions, we performed localisation and ROS burst activity assays. For this, we chose the orthologs of Rip1 from *S. scitamineum* (SPSC_05323), *U. hordei* (UHOR_13428), *U. bromivora* (UBRO_13428) and *M. pennsylvanicum* (BN887_05943) (Supplementary Fig. 2B). *N. benthamiana* plants were used to transiently express these different Rip1 orthologs without their endogenous signal peptide as mCherry fusion constructs. All ortholog constructs were successfully expressed in *N. benthamiana* as confirmed by western blot (Supplementary Fig. 2C). Confocal microscopy illustrated a localisation within the nucleus as well as the cytoplasm for all of the tested Rip1 orthologs (Fig. 2A). Moreover, the ability of ROS burst suppression after challenging with flg22 was observed among all tested orthologs, except for the *M. pennsylvanicum* derived Rip1 ortholog, whose ROS levels were comparable to that of mCherry control plants (Fig. 2B).

In order to determine if there is a critical region responsible for the ROS suppression, we first designed several *U. maydis* Rip1 truncation versions using predicted structural positions of α-helixes as benchmarks with CLC Main Workbench 8.1 (Supplementary Fig. 2D). While full length Rip1 was able to suppress ROS burst after treatment with the flg22 peptide in infiltrated *N. benthamiana* plants, all Rip1 truncation versions completely lost their ability to decrease the plant ROS accumulation, showing ROS levels similar to the mCherry control (Supplementary Fig. 2E). Protein integrity was confirmed by western blot (Supplementary Fig. 2F). Since the Rip1 ortholog from *M. pennsylvanicum* was the only protein unable to suppress ROS burst in plants, we next

investigated whether protein sequence comparisons between all tested orthologs might unravel cryptic motifs essential for ROS suppression functionality. Indeed, our alignment revealed a K-H-L-P-D-L-S-$R_{(0,1)}$-P motif, designated as **Ri**p1 **F**unctiona**l** (RIFL) motif, preserved at the C-terminus among all orthologs except for *M. pennsylvanicum*, which harbors a truncated, degenerated sequence at this position (Fig. 2C). To determine the importance of this motif for ROS burst suppression, we generated motif deletion and insertion mutations using *Um*Rip1 or *Mp*Rip1, respectively (Fig. 2D). We expressed the aforementioned constructs in *N. benthamiana* and tested their ability to suppress ROS burst. Plants expressing free mCherry were used as control. Protein integrity and localisation of tested constructs in *N. benthamiana* were confirmed by western blot and confocal microscopy, respectively (Supplementary Fig. 2G and 2H). Confocal microscopy analysis revealed that the RIFL motif does not influence the localisation of Rip1-mCherry (Supplementary Fig. 2H). Strikingly, we observed that Rip1 lacking the RIFL motif failed to suppress ROS burst, whereas an insertion of the RIFL motif at the C-terminus of *Mp*Rip1 was sufficient to endow its ROS burst suppression function (Fig. 2D). Fusion of RIFL alone to mCherry did not lead to ROS burst suppression, indicating that additional Rip1 related sequence features are required for its ROS burst suppressive function. Taken together, our results demonstrate that the C-terminal RIFL motif is necessary for ROS burst suppressive activity of Rip1 and that one can restore this PTI-suppressive function in the *M. pennsylvanicum* ortholog by fusing the RIFL-motif to it.

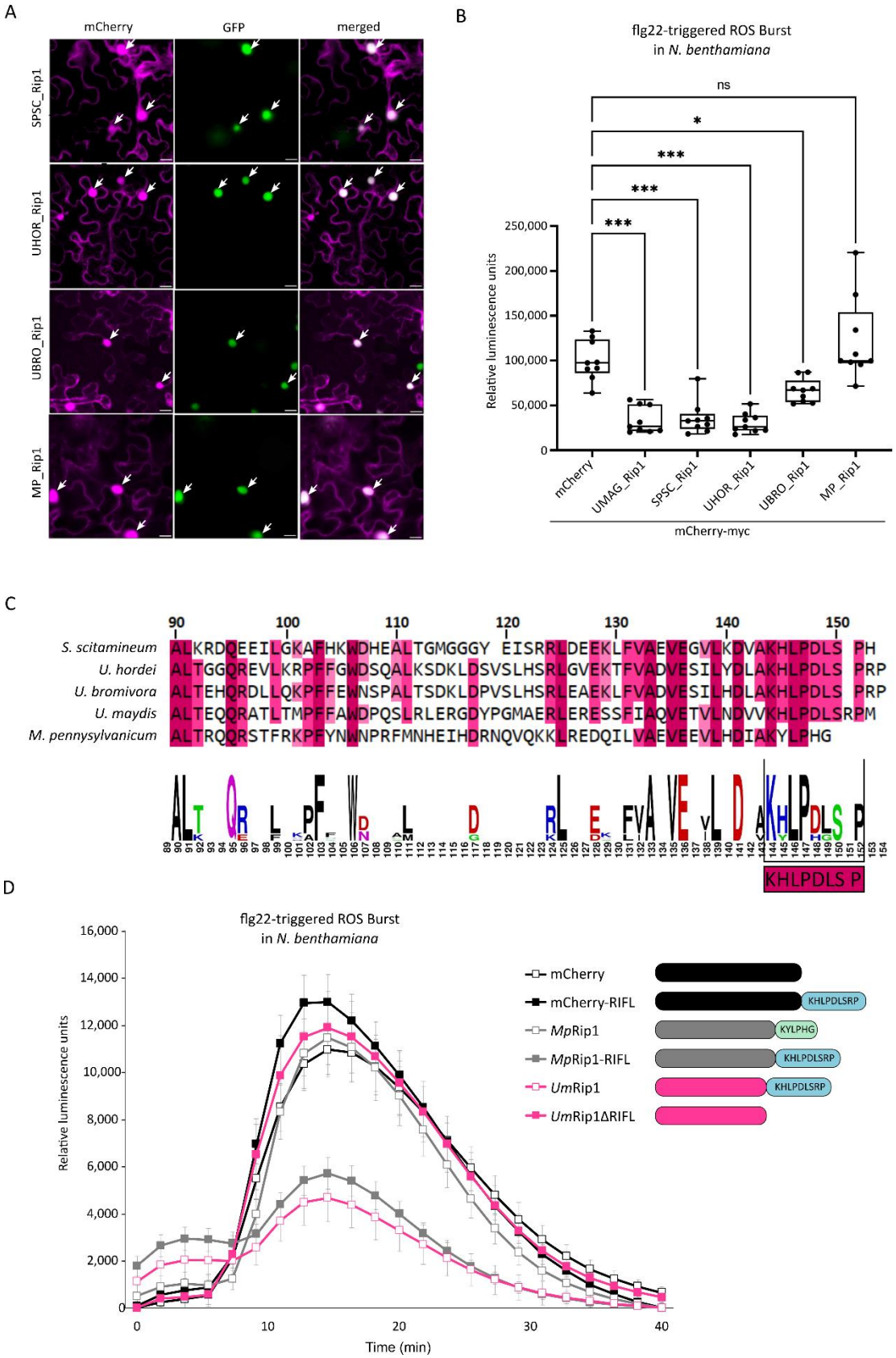

Figure 2: Rip1 orthologs suppress ROS burst in *N. benthamiana* plants. A. Localisation of different Rip1 orthologs in *N. benthamiana* from *Sporisorium scitamineum* (SPSC_05323) (host plant sugarcane), *Ustilago hordei* (UHOR_13428) (host plant barley), *Ustilago bromivora* (UBRO_13428) (host plant Brachypodium) and *Melanopsichium pennsylvanicum*

(BN887_05943) (host plant Polygonaceae). Orthologs were fused to myc-mCherry, co-expressed with P35S::GFP-NLS and localisation was assessed by confocal microscopy. Localisation was observed in the nucleus and the cytoplasm for all orthologs. Left panel: mCherry, middle panel: GFP, right panel: merged mCherry and GFP. Arrows exemplarily mark plant cell nuclei. Scale bar = 20 µm. **B.** *N. benthamiana* plants expressing different Rip1 orthologs driven by the constitutive promoter 35S were assessed for ROS activity. Box plots represent the area under the ROS burst curve after challenging with PAMP-flg22 monitored over 40 minutes based on a luminescence assay. All orthologs of Rip1 were able to significantly suppress ROS burst, except plants expressing *Mp*Rip1. Shown data is a pool of three biological replicates calculated as area under the curve; n=9. Asterisks indicate statistically significant differences to the control (ns: non-significant, * $p<0.05$, *** $p<0.05$, one-way ANOVA followed by Tukey's test). **C.** Part of the C-terminal protein sequence Clustal alignment of Rip1 orthologs. Different shaded colors indicate global percentage identities of 3 or more identical aa among the proteins. Highly conserved C-terminal region present for all, but *Mp*Rip1 is highlighted with black box. Numbers on top indicate protein length in aa based on signal peptide deleted sequences. **D.** Schematic representation of different deletion and insertion mutation constructs of Rip1 and *Mp*Rip1. The RIFL motif (KHLPDLSRP) is important for the ROS burst suppressive activity of Rip1 *in planta*. Expression of *Um*Rip1 lacking its endogenous C-terminal RIFL motif shows similar ROS burst activity levels as mCherry control plants. On the contrary, plants expressing *Mp*Rip1 with a C-terminal RIFL motif replacement show ROS-burst suppressive activity in comparison to the control plants. Curves represent plant ROS-burst levels after challenging with flg22 monitored over 40 minutes based on a luminescence assay. Shown data is a pool of three biological replicates; Error bars represent SE, n=9.

Rip1 targets maize LOX3 (Zmlox3), a negative regulator of ROS generation

As Rip1 likely targets a conserved plant pathway due to its ROS-burst suppressive activity in maize as well as in the dicot *N. benthamiana,* we made use of the easy accessibility of the latter model organism to perform co-immunoprecipitation-coupled mass spectrometry in order to identify potential Rip1 plant interactors. For this purpose, P35S::Rip1$_{27-166}$-mCherry- myc was expressed in *N. benthamiana* leaves, pulled down with anti-myc magnetic beads and subjected to mass spectrometry for protein complex identification. Plants expressing P35S::mCherry-mCherry-myc were used as control. Protein integrity was assessed beforehand by western blot (Supplementary Fig. 3A). Co-immunoprecipitation experiments were performed twice and MS- identified proteins were combined for the analysis (Supplementary Fig. 3B). Interestingly, the top hit of our results was a protein of approximately 95 kDa in weight, identified on the SGN database (Sol Genomics Network) as LOX6 (Niben101Scf01434g03006.1). Previous studies indicate that LOXes are induced during plant-pathogen interactions and are involved in plant PTI response, which prompted us to further investigate its connection with Rip1 (Doehlemann et al., 2008;

Pathi et al., 2020). Using BLASTP, we identified the closest homolog of Niben101Scf01434g03006.1 in maize to be LOX 3 (NP_001105515.1) with 60 percent protein identity (Supplementary Fig. 3C and 3D). Next, we tested for the ability of Rip1 to directly interact with Zmlox3 using a directed yeast two-hybrid assay. A direct interaction between Rip1 and Zmlox3 was confirmed in this system (Fig. 3a). Further, to confirm this interaction, we performed co-immunoprecipitation in *N. benthamiana* leaves by co-expressing P35S::Rip1$_{27\text{-}166}$-mCherry-myc and P35S::Zmlox3-GFP. We extracted total proteins from leaves expressing either P35S::Rip1$_{27\text{-}166}$-mCherry-myc or P35S::mCherry-mCherry-myc (control) and P35S::Zmlox3-GFP and immunoprecipitated myc-tagged proteins with anti-myc magnetic beads. Zmlox3 protein co-immunoprecipitated with P35S::Rip1$_{27\text{-}166}$-mCherry-myc but not P35S::mCherry-mCherry-myc when observed using Western Blot (Fig. 3B) that utilized an anti-lox antibody which specifically binds to Zmlox3 (Supplementary Fig. 3E).

As Rip1 suppresses PTI-responses, we tested the role of its interacting LOX on PAMP-triggered ROS accumulation by virus induced gene silencing (VIGS) followed by PAMP-induced ROS measurements. For this purpose, we used a Tobacco rattle virus (TRV) based silencing vector targeting a unique region of Nblox6 in *N. benthamiana* (Supplementary Fig. 2F) (Fernandez-Pozo et al., 2015). Successful VIGS of Nblox6 was determined by qPCR showing reduced expression levels of Nblox6 in silenced plants (Supplementary Fig. 2G). Four weeks post infection (wpi), tobacco plants show neither cell death indication in leaves nor any other obvious phenotypical changes in comparison to the control plants (Supplementary Fig. 2H). Later, VIGS plants were challenged with flg22 and ROS accumulation was monitored by a luminol-based assay. Nblox6 silenced plants showed significantly higher accumulation of ROS compared to control plants (Supplementary Fig. 2I) indicating a negative role of Nblox6 in ROS generation.

In order to investigate if the maize LOX has a similar role in PAMP-triggered ROS-accumulation, a transposon-mutagenized mutant maize line was used (Gao et al., 2007). The maize *lox3-4* mutant line showed significantly higher ROS levels upon PAMP flg22-treatment compared to wild type B73 (Fig. 3C). Altogether, these results indicate a conserved function of maize LOX3 and its *N. benthamiana* ortholog Nblox6 as negative players of PAMP-triggered apoplastic ROS generation.

To test these results further, we overexpressed Zmlox3 under the strong constitutive 35S promoter (P_{35S}::Zmlox3-GFP) in *N. benthamiana* leaves and challenged them with flg22-PAMP to monitor ROS generation. We fused Zmlox3 with a C-terminal tag leading to an enzymatically inactive protein since the conserved C-terminus in all LOXs known so far is part of the active center (Newcomer and Brash, 2015). Remarkably, overexpression of enzymatically inactive Zmlox3 in *N. benthamiana* plants led to significantly reduced levels of ROS accumulation compared to control plants (Fig. 3D). Similar results were also observed by overexpression of endogenous C-terminally tagged Nblox6 in *N. benthamiana* under the 35S promoter (Supplementary Fig. 3J).

To elucidate whether there is a correlation between Zmlox3, Rip1 and plant ROS activity, we co-expressed Zmlox3 and $Rip1_{27\text{-}166}$ in *N. benthamiana* and monitored the ROS accumulation after flg22-PAMP triggered ROS burst. By co-expressing both interacting proteins in the plant cell, we observed that ROS-burst suppression activity was strengthened significantly in the co-expressing plants (Fig. 3D).

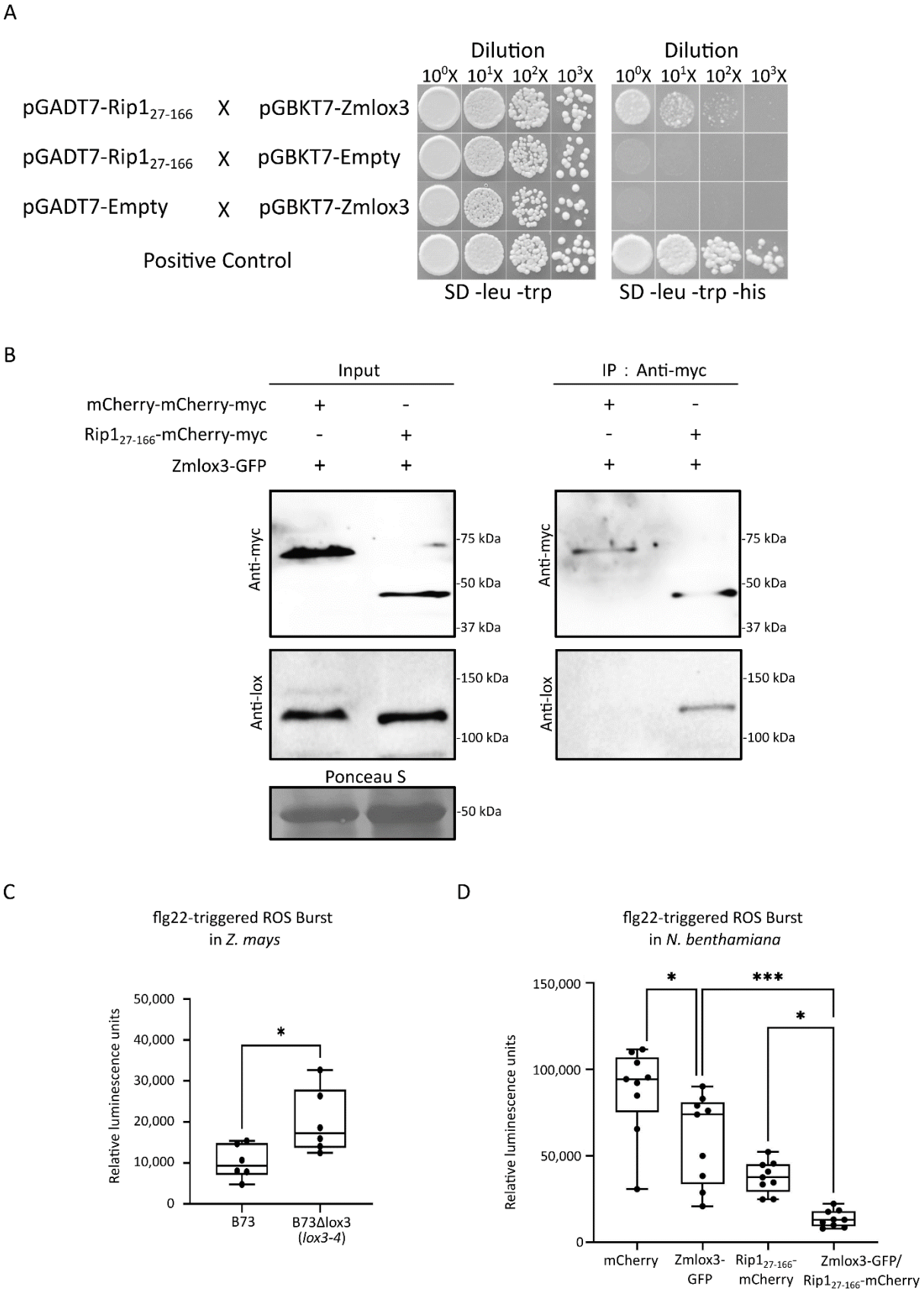

Figure 3: Rip1 targets maize LOX3 (Zmlox3), a negative regulator of PAMP-triggered ROS-burst. A. Direct interaction of Rip1 and Zmlox3 in a Yeast-two-Hybrid assay. Zmlox3

was cloned into pGBKT7 bait vectors and transformed into the yeast strain Ah109, whereas Rip1 was cloned into pGADT7 activation vector and transformed into the yeast strain Y187. Diploid yeast after mating, containing both plasmids, were dropped on selective synthetic dropout media (SD) and yeast growth was monitored 4 days after spotting. Columns in each panel represent serial decimal dilutions. Positive control represents a laboratory internal reference of two strongly interacting proteins (other *U. maydis* effector and maize plant protein, unpublished). The experiment was repeated 3 times independently with comparable results. **B.** Co-immunoprecipitation (Co-IP) assay showing that Rip1 interacts with ZmLox3 in *N. benthamiana*. We co-expressed P35S:Rip1$_{27\text{-}166}$-mCherry-myc or P35S:mCherry-mCherry-myc (control) and P35S::Zmlox3-GFP in *N. benthamiana* leaves and performed a Co-IP using anti-myc antibody. Western blot shows that Zmlox3 detected with Zmlox3-specific antibody were co-purified with P35S:Rip1$_{27\text{-}166}$-mCherry-myc but not with P35S:mCherry-mCherry-myc **C.** Knock-out lines of maize *lox3* (*lox3-4* mutant, Gao et *al.,* 2007) show elevated ROS levels after flg22 treatment. Mutant lines of *lox3* were grown for 14 days before leaves were used in a flg22-PAMP triggered ROS burst assay. ROS accumulation was monitored over 40 minutes with a luminescence-based assay. As control maize plants of the B73 accession were used. Data is shown as box plots for the area under the curve of two pooled biological replicates, n=6/replicate. Significant statistical differences to control plants: Student t-test, * $p<0.05$. **D.** ROS burst inhibition effects are synergistically enhanced in the presence of both, expressed Zmlox3 and Rip1 in *N. benthamiana*. Plants expressing P35S::Zmlox3-GFP, P35S::Rip1$_{27\text{-}166}$-mCherry or both constructs in combination were infiltrated into *N. benthamiana* and flg22 triggered ROS burst was monitored over 40 minutes with a luminescence based assay. The ROS burst suppressing activities of single infiltrated Zmlox3 and Rip1 overexpression constructs were further significantly enhanced by co-infiltration of both constructs. The OD_{600} for Zmlox3 was set to 0.2 and for Rip1 to 0.05, respectively. Data is shown as box plots for the area under the curve of three pooled biological replicates, n=9/replicate. Significant statistical differences of P35S::Zmlox3-GFP to control plants P35S::mCherry: Student t-test, * $p<0.05$. Significant statistical differences of P35S::Zmlox3-GFP and P35S::Rip1$_{27\text{-}166}$-mCherry to P35S::Zmlox3-GFP/ P35S::Rip1$_{27\text{-}166}$-mCherry: * $p<0.05$,*** $p<0.05$, one-way ANOVA followed by Tukey's test.

Relocalisation of enzymatically inactive Zmlox3 into the nucleus increases its ROS suppressive activity

Following the observation of elevated ROS suppression in *N. benthamiana* plants expressing C-terminally tagged Zmlox3 and Rip1, we decided to resolve the localisation of Zmlox3 and Rip1 in plant cells. Evaluation of *N. benthamiana* and *Z. mays* plant tissue expressing P35S::ZmLox3-GFP co-infiltrated with P35S::mCherry, which marks plant nuclei and cytoplasm, showed ZmLox3 to be localized mainly in the cytosol, while only faint or no Zmlox3 derived fluorescent signals could be observed within the plant nucleus for both plant species (Fig. 4A, Supplementary Fig. 4A and. 4B). Intriguingly, when co-expressing Zmlox3-GFP together with the nucleo-cytoplasmic Rip1-mCherry in these plants, a relocalisation of Zmlox3 into the plant nuclei was revealed throughout the transformed tissues (Fig. 4A, Fig. 4B and

Supplementary Fig. 4A). To further test if Rip1 actively directs Zmlox3 into the plant nucleus, we co-expressed a NES tagged version of Rip1 with Zmlox3 in *N. benthamiana.* Our results show that Zmlox3 is no longer relocalizing into the nucleus upon the restriction of Rip1 to the cytoplasm (Supplementary Fig. 4C). Consequently, Rip1 was unable to leverage Zmlox3 to maximize ROS burst suppression (Supplementary Fig 4D). To verify the protein integrity of the used constructs, a western blot was performed (Supplementary Fig. 4E).

Given the results so far, the next line of inquiry was to determine whether there might be a connection between the observed Rip1-induced nuclear translocation of Zmlox3 and its previously established involvement in plant immunity (Constantino et al., 2013, p. 3; Gao et al., 2009, 2007; Pathi et al., 2020). To get more insight into a possible localisation-dependent Zmlox3 effect on plant immunity, we performed a ROS burst activity assessment of subcellularly mis-localized, terminally tagged Zmlox3 proteins. For this purpose, we made use of MYR, NLS and NES tags by fusing them to the coding region of Zmlox3 as mentioned before. After confirming successful Zmlox3 mis-localisations (Supplementary Fig. 4F and Supplementary Fig. 4I), we performed ROS burst assays in *N. benthamiana* as described before. Indeed, the specific targeting of C-terminally tagged ZmLox3 into the plant nucleus led to significantly higher ROS burst suppressions compared to plants expressing either free mCherry or MYR and NES Zmlox3 fusions (Fig. 4C). To follow this up, we used a glucocorticoid receptor (GR)-based inducible gene expression system, which allows for Dexamethasone-induced nuclear translocation of respective fusion proteins. We fused the GR steroid-binding domain C-terminally to ZmLox3 or mCherry as control, driven by the constitutive 35S promoter and expressed these constructs in *N. benthamiana*. The GR steroid-binding domain preserves the constitutively expressed Zmlox3 or mCherry proteins within the cytoplasm. Upon application of Dexamethasone (DEX), the translocation of Zmlox3-GR or mCherry-GR proteins into the nucleus is triggered (Supplementary Fig. 4G and Supplementary Fig. 4H) (Brockmann et al., 2001). Plants expressing P35S::Zmlox3-GR treated with DEX showed significantly higher ROS-suppression activities compared to non-treated DEX plants or mCherry control plants, confirming the importance of a nuclear localized Zmlox3 for its effect in ROS burst suppression (Fig. 4D).

To test if C-terminally tagged versions of Zmlox3 are showing any detectable LOX activity, we expressed ZmLox3 c-terminally fused to mCherry, mCherry-NLS or mCherry-NES and N-terminally with a 6xHis-tag in *Escherichia coli* and affinity purified the proteins to be tested in LOX assays. Whereas the N-terminally tagged control ZmLox3 shows activity to both substrates, α-linolenic and linoleic acid, no such activity could be detected *in vitro* for any of the C-terminally tagged versions of Zmlox3 (Supplemental Fig. 4J). Taking the Zmlox3 mislocalisation, ROS-burst assay results and the enzymatic activity assays together, this indicates that the PTI-suppressive property of native Zmlox3 is not connected to its enzymatic activity in the 9-LOX pathway. Furthermore, our results demonstrate, that a nuclear localisation of Zmlox3 is critical and beneficial for its ROS suppression activity.

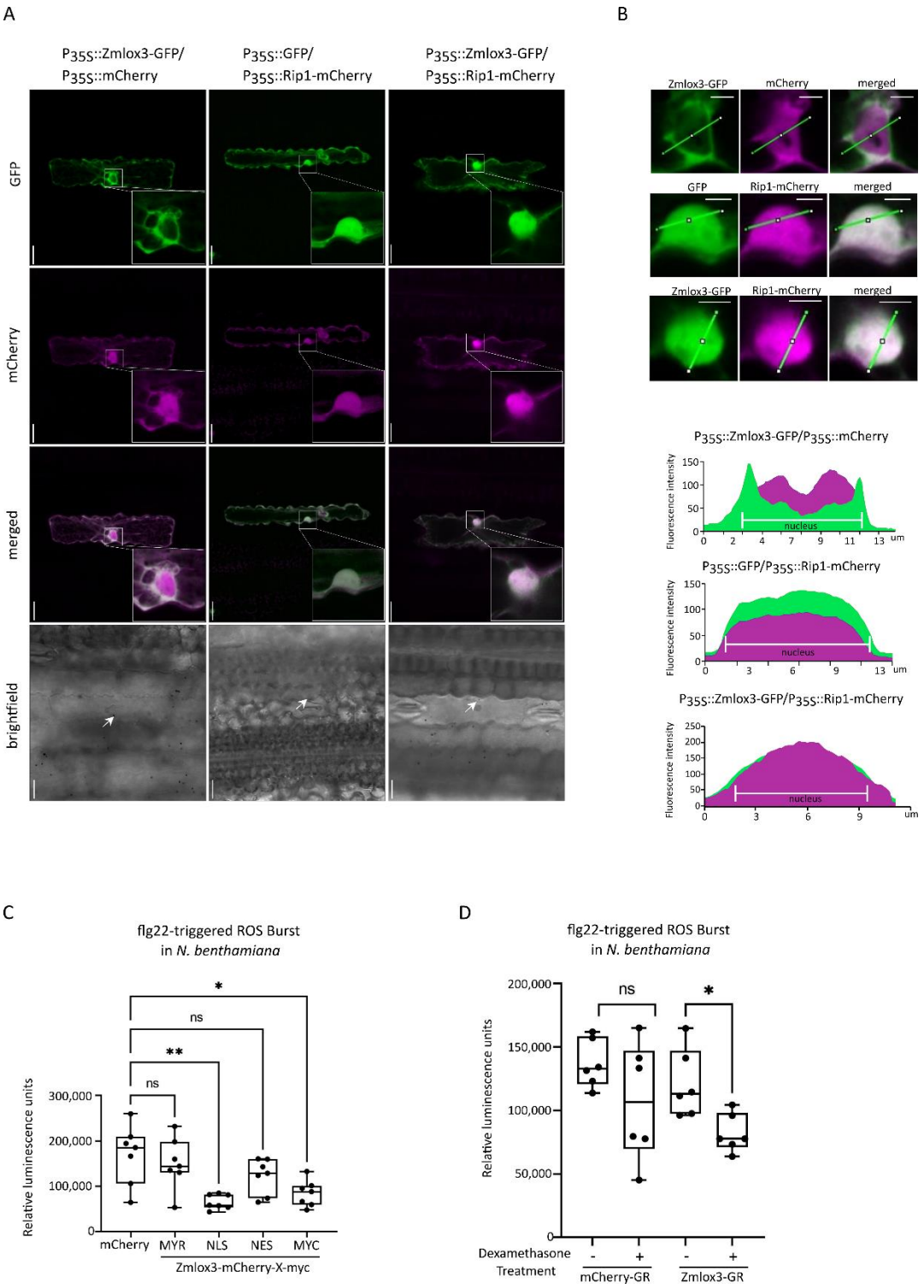

Figure 4: *Zmlox3* is translocated into the nucleus by Rip1 co-expression to increase its ROS suppressive activity. A. Zmlox3 translocalizes into the nucleus in the presence of Rip1 in *Z. mays* plants. Full length Zmlox3 was fused to GFP and Rip1 lacking its signal peptide was fused to mCherry under control of the cauliflower mosaic virus 35S promoter. P35S::mCherry and P35S::GFP were used as controls for the co-localisation assay, respectively. *Z. mays* leaves were co-bombarded with P35S::Zmlox3-GFP/ P35S::mCherry, P35S::Rip1$_{27\text{-}166}$-mCherry/ P35S::GFP or P35S::Zmlox3-GFP/ P35S::Rip1$_{27\text{-}166}$-mCherry and after 2 days fluorescence signals were observed by confocal microscopy. Upper panel: GFP, Upper middle panel: mCherry, Lower middle panel: merged mCherry and GFP, Lower panel:

brightfield. Pictures are merged z-stack projections. Inlets represent magnified areas of plant cell nuclei within the pictures. Arrows indicate position of the plant cell nucleus. Scale bar = 20 µm. **B.** Fluorescence intensity profiles of mCherry and GFP channel pictures along transection lines (green) at nuclear regions are visualized as relative grey values (plots). Purple plot areas represent mCherry intensity levels, green plot areas represent GFP intensity levels. Zmlox3 in the presence of Rip1 shows increased nuclear GFP signals, while GFP intensities decrease within the nucleus when Zmlox3 is co-expressed with mCherry control. Pictures show a single plane of a z-stack from a. Scale bar = 5 µm. **C.** Subcellular mis-localisation ROS-burst assay of Zmlox3 in *N. benthamiana* using different localisation tags (MYR, NLS and NES). Highest ROS burst suppression activity was identified in nuclear targeted ZmLox3 plants. Box plots represent the area under the ROS burst curve after challenging with PAMP-flg22 monitored over 40 minutes based on a luminescence assay. Shown data is a pool of three biological replicates; n=7. Asterisks indicate statistically significant differences from the control (ns: non-significant, * $p<0.05$, ** $p<0.05$, one-way ANOVA followed by Tukey's test). **D.** Glucocorticoid system-based nuclear translocation of Zmlox3 enables ROS burst suppression. *N. benthamiana* plants were infiltrated with P35S::Zmlox3 or P35S::mCherry (control) coupled to a binding domain of a glucocorticoid receptor (GR) and were treated with DEX (dexamethasone) or H_2O after 24 hours. Box plots represent the area under the ROS burst curve monitored over 40 minutes with a luminescence-based assay. Data is shown as a pool of two biological replicates; n=6. Significant statistical differences of P35S::Zmlox3-GR or P35S::mCherry-GR treated with DEX to control plants P35S::Zmlox3-GR or P35S::mCherry-GR treated with H_2O. Student t-test, ns: non-significant, * $p<0.05$.

Inactivation of Zmlox3 increases susceptibility of maize plants towards Ustilago maydis in the absence of Rip1

In our previous study, we showed that Zmlox3 is a susceptibility factor in the *U. maydis*/maize interaction, hence *zmlox3* mutant maize shows moderate resistance to *U. maydis* (Pathi et al., 2020). Therefore, we next investigated whether the absence of Rip1 affects this increased resistance of lox3 mutation. Maize seedlings of B73Δlox3 (*lox3-4::Mu*) were infected with the solopathogenic strain SG200 or the respective deletion strain SG200Δ*rip1*. We also included the B73 maize seedling infection sets as the wild-type control since B73 is the recurrent parent for lox3-4 mutant at the BC7 genetic stage. As expected, in B73, fungal disease scoring (Fig. 5A) showed, that the symptoms induced by SG200Δ*rip1* were not different from those induced by SG200, which coincides with the ipool-seq results (Uhse et al., 2018). On the contrary, infected maize seedlings lacking *lox3* showed significantly less infection symptoms compared to the B73 wild type, which supports the results of our previous studies. Remarkably, rip1 deletion strains infecting *lox3* mutant maize seedlings gained back largely their virulence, implying a Rip1 co-dependency for the previously observed partial resistance phenotype of lox3 mutant. We further generated a complementation strain

of SG200Δ*rip1* by ectopic integration of the *rip1* gene under the native rip1 promoter into the well described *U. maydis ip* locus and used it for infection of the B73Δlox3 mutant (Loubradou et al., 2001). Comparable to infections with the fungal progenitor strain, again significantly less infection symptoms were present, confirming that the aforementioned effects of the SG200Δ*rip1* mutant strain on B73Δlox3 mutant are Rip1-specific. The ability of the SG200Δ*rip1* mutant strain to still penetrate epidermal cells in B73 and B73Δ*lox3* were confirmed by the microscopic analysis (Fig. 5B). Taken together, these results indicate, that Rip1 without its plant target Zmlox3, is not able to promote full virulence, in contrast, that its presence is a requirement for the observed reduced susceptibility of B73Δ*lox3* maize to *U. maydis* infection. .

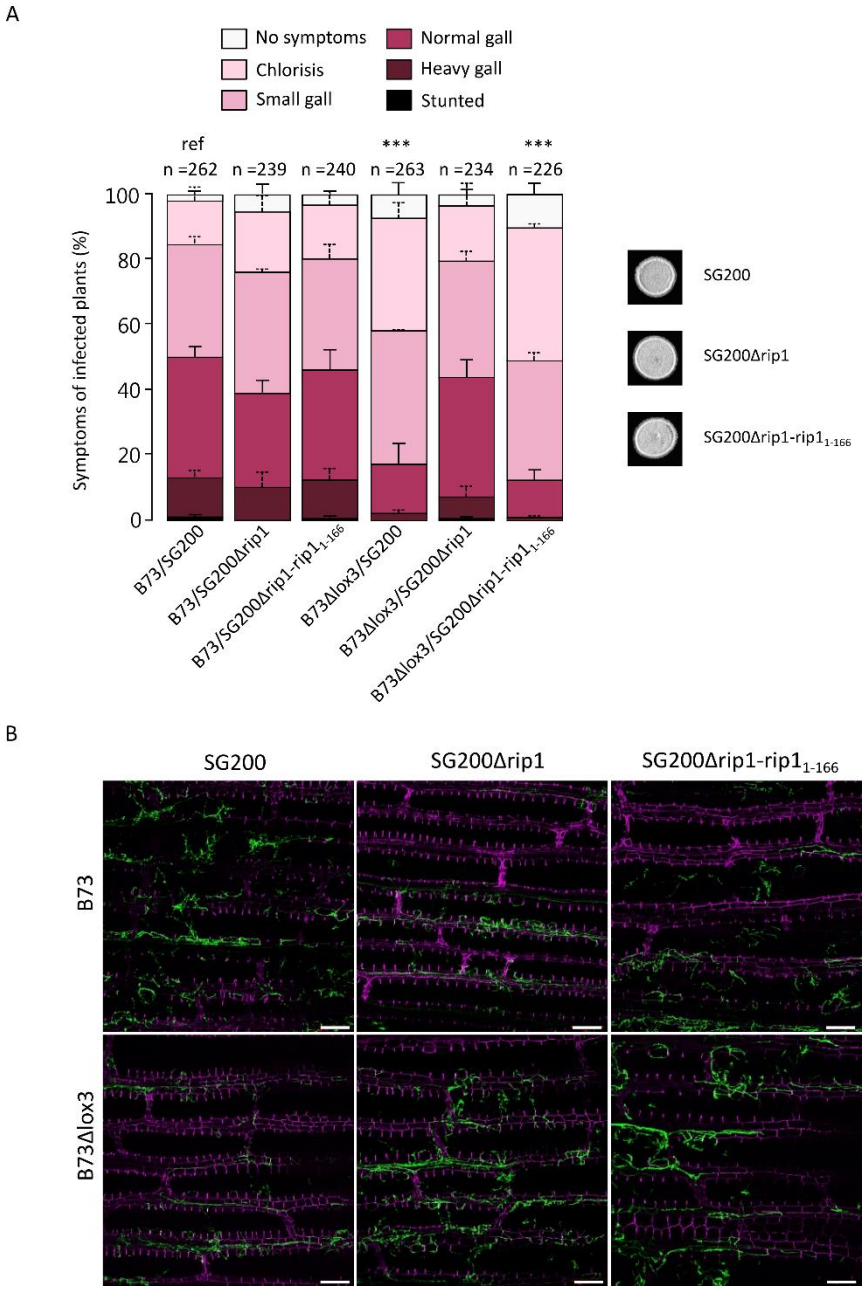

Figure 5: ***Presence of rip1 in Zmlox3 mutant maize plants is causative for the reduced host colonization.*** **A.** Virulence assays carried out in 7 days old maize seedlings cv. B73 and B73Δ*Lox3* (Zmlox3 deletion mutant, *lox3-4*) infected with the *U. maydis* progenitor strain SG200, SG200Δ*rip1* (*rip1* deletion strain) and the complementation strain of SG200Δ*rip1* (SG200Δ*rip1-rip1*$_{1\text{-}166}$). The complementation strain was generated by using a full length Rip1 expression construct under the native Rip1 promoter. Symptom rating of *U. maydis* SG200Δ*rip1* strain showed no significant virulence defect in comparison to the progenitor strain SG200 in maize cv. B73. Significantly less disease symptoms, however, were observed in maize seedlings cv. B73Δ*Lox3* infected with SG200 and the complementation strain SG200Δ*rip1-rip1. U. maydis* SG200Δ*rip1* caused in B73Δ*Lox3* infected maize plants nearly full symptoms, implicating a negative effect of Rip1 on virulence in the absence of ZmLox3. Data represent mean ± SD from three independent experiments, n= total number of scored plants. Significant differences between strains were analyzed by the Fisher's exact test and multiple testing correction was performed using Benjamin-Hochberg. Asterisks indicate statistical significance. (*** p<0.0001). Controls (B73 and B73Δlox3 infected with SG200) of this experiment were done in colaborations and used in the publication Pathi et al. 2021. **B.** Microscopic analysis of Rip1 virulence phenotype in B73 and B73Δ*Lox3*. Maize plants of cv. B73 were infected with the progenitor strain SG200, the deletion strain SG200Δ*rip1* or the complementation strain SG200Δ*rip1-rip1*$_{1\text{-}166}$, and harvested at 3 dpi. Pictures show the intracellular proliferation of *U. maydis* in epidermal maize cells. Infected leaf tissue was stained with WGA-AlexaFluor488 (green) to visualize fungal chitin and propidium iodide (red) to observe plant cell walls. Pictures show that the progenitor strain SG200, the deletion strain SG200Δrip1 and the complementation strain SG200Δrip1-rip1$_{1\text{-}166}$ were able to penetrate inside maize tissue from cv. B73 and cv. B73 B73Δ*Lox3.* Z-stack pictures were made with confocal microscopy. Scale bar = 100 µm.

Discussion

The eternal co-evolutionary battle between plants and their pathogens led to tightly interwoven host receptor-driven recognition and pathogen effector-driven signaling-suppression events. Plants evolved a versatile repertoire of membrane bound and cytosolic receptors that recognize conserved pathogen associated molecular patterns or effectors and their activities (Zhou and Zhang, 2020). Pathogen effectomes on the other hand, are selected to suppress both PAMP-triggered (PTI) and Effector-triggered immunity (ETI) responses to ensure a compatible interaction. In both, PTI as well as in ETI-responses, reactive oxygene species (ROS) play a critical role leading either to the transient ROS-burst as part of early signaling or culminate in a hypersensitive response, a programmed cell-death to restrict systemic spread of the pathogen (Jwa and Hwang, 2017). Due to its relevance in defence, it is not surprising that *U. maydis* evolved numerous functionally redundant effectors that suppress the accumulation of ROS. This is exemplified by the Pleiades, an entire cluster of effectors, nine members

of which were shown to suppress PAMP-triggered ROS-burst *in planta* in different mechanisms (Navarrete et al., 2021b). The fact that many *U. maydis* effectors target PTI-responses like the PAMP-triggered ROS-burst explains the lack of a strong virulence defect upon Rip1-deletion due to functional redundancy. More surprising was the discovery, that the strong reduction in fungal virulence upon Zmlox3 mutant maize infections could be rescued by a compensatory removal of *rip1* on the pathogen side. One possible explanation of this observation could be that the effector Rip1 itself or its activity leads to the induction of host defence responses in maize, whereby Rip1 binding to Zmlox3 is necessary to suppress ROS-mediated defense. In this case ZmLox3 would be having a role as a negative regulator of Rip1 effector-triggered defense in the maize/*U. maydis* interaction. Zmlox3 has been previously shown to be involved in either susceptibility or resistance in maize in a pathogen-dependent manner. Whereas Gao et *al.*, 2008 and 2009 demonstrated a higher susceptibility of *lox3* maize mutants to root knot nematodes and to fungi like *Aspergillus flavus and Aspergillus nidulans*, Gao et *al.,* 2007 and 2009 as well as Pathi et *al.,* 2020 demonstrate for various fungal pathogens including *Fusarium verticillioides* (Gao et al., 2007)*, Colletotrichum graminicola* (Gao et al., 2007)*, Cochliobolus heterostrophus* (Gao et al., 2007)*, Exserohilum spp* (Isakeit et al., 2007) and *U. maydis* (Pathi et al., 2020) an increase of resistance for plants lacking Zmlox3. Additionally, Zmlox3 was recently shown to be a major negative regulator of induced systemic responses triggered by *Trichoderma virens* colonization of roots (Constantino et al., 2013; Wang et al., 2020). This implies that the outcomes of LOX-governed host-pathogen interactions are pathogen-specific. However, in the case of the *U. maydis*/maize interaction, Zmlox3 is a susceptibility factor. In the case of the Aspergillus/maize interaction, there were indication found of oxylipin signaling interplay between the host and the fungus, leading to the speculation of signaling mimicry and respective interference (Gao et al., 2009). In the case of *U. maydis/Zea mays*, considering the necessity of the presence of Zmlox3 to suppress Rip1-dependent reduction of susceptibility of maize to *U. maydis*, such a signaling mimicry scenario is not likely.

Moreover, we show that *U. maydis* secretes the translocated effector protein, Rip1, to suppress PAMP-triggered ROS production in maize. This is partly achieved by direct interaction with Zmlox3 and the resulting relocalization of this enzyme from cytoplasm to nucleus. Importantly, Rip1 has obviously more than one cellular target by which

ROS-burst suppression is achieved, as also cytosolic retention experiments still show a saturated capacity to suppress ROS-burst *in planta* by MYR-Rip1 and Rip1-NES. This feature of multifunctionality is shared with several other effectors. One recently published example for *U. maydis* is Nkd1. This effector targets Topless-like proteins (TPLs) and induces auxin signaling to suppresses PAMP-triggered ROS-burst. On the other hand, its deletion causes a virulence defect that is not linked to its interaction with TPLs (Navarrete et al., 2021a). Examples of other multifunctional effectors are Avr3a from the oomycete *Phytophtora infestans* or AvrPiz-t from the rice blast fungus *Magnaporthe oryzae* (He et al., 2020).

The finding that ZmLox3 ROS-burst suppressing activity is not linked with its enzymatic LOX activity, but with the forced nuclear relocalisation opens a new field in LOX research. Currently one can only deduce, that a direct ROS-buffering function of the LOX products, that suppresses the apoplastic ROS-burst can be excluded in this case. However, it is tempting to speculate, that the N-terminal C2-like-calcium binding domain of Zmlox3 might play a role in this process (Newcomer and Brash, 2015).

Zmlox3-GFP predominately localized to the cytoplasm when expressed in maize and tobacco plants. This type of localization pattern was also described for several members and isoforms of the maize 9-Lox family in maize and *A. thaliana* roots (Tolley et al., 2018). Interestingly, by using a universal anti-LOX antibody that recognizes multiple types of LOX proteins, Demenchenko et *al.* (2011) reported a strong nuclear Lox protein localization next to the infected plant cells specifically in the nitrogen fixation zone in nodules produced by symbiotic rhizobia in the roots of the legume plant *Medicago truncatula* (Demchenko et al., 2012). As symbiotic interactions also rely on effector activities (Daguerre et al., 2016), one possible explanation for the observed relocalisation of the LOX proteins could be bacterial effector activities similar to Rip1 (Feussner et al., 1995). Alternatively, nuclear relocalisation could be triggered by plant-specific developmental or external cues. Searching for those, we tested various abiotic stresses and hormone treatments (data not shown) but could not detect nuclear localizations of fluorescent protein-tagged Zmlox3 *in planta*. An active re-localisation of lipoxygenases into the nucleus has been reported in mammalian organisms (Brock et al., 1994; Luo et al., 2003). One type of LOX, the immunity and defense related 5-lipoxygenase (5-LO), possess the ability of shuttling between the cytoplasm and the nucleus, thereby regulating the leukotriene biosynthesis in

response to inflammatory or allergic diseases. It is suggested that it may be the result of the phosphorylation status at the site of its NES motif or indirectly by interactions with intermediate protein partner in a Ca^{2+}-dependent manner (Flamand et al., 2009; Hammarberg et al., 2000). As relocalisation of Zmlox3 to the nucleus occurs only if also Rip1 is not constantly exported by a nuclear export sequence, it is likely that Rip1 carries Zmlox3 in a complex into the nucleus. An alternative hypothesis is that Rip1 might induce posttranslational modification triggering Zmlox3 nuclear relocalisation.

Previous studies have reported that Zmlox3 is mainly expressed in roots and tassel but only weakly in leaf tissue (Constantino et al., 2013). These data contradict with the observation that *U. maydis* is using Zmlox3 as a susceptibility factor (Pathi et al., 2020) as this fungal pathogen infects only the aerial parts of the plant. On the other hand, transcriptomic timecourse experiments demonstrated that *U. maydis* induces Zmlox3 strongly upon infection of maize seedlings (Doehlemann et al., 2008) and makes it therefore at the infection site available for further manipulation by Rip1 during the biotrophic phase as presented here.

Rip1 effectors harbor a terminal RIFL motif required for ROS burst suppression

By testing four *U. maydis* Rip1 orthologs from other smut fungal species, we identified three additional Rip1-like proteins that were able to effectively suppress plant ROS burst. All of them belong to fungal genera that infect monocot hosts. In contrast, the Rip1 ortholog from *M. pennsylvanicum*, which contains a similar overall protein identity with the others, did not exert any ROS suppressive function. Intriguingly, *M. pennsylvanicum* is a pathogen that infects dicot plants of the Polygonaceae family and *Mp*Rip1 does not possess a predicted signal peptide. This provides evidence for a putative neo-functionalization of *Mp*Rip1 within *M. pennsylvanicum*. A comparative analysis of all Rip1 orthologous sequences revealed a C-terminal K-H-L-P-D-L-S-$R_{(0,1)}$-P motif, named as RIFL motif, as an essential part of the Rip1 mediated ROS burst suppression function that is present in all analyzed monocot-infecting sequenced smut-species analyzed, but absent in *M. pennsylvanicum*. Surprisingly, fusion of RIFL to *Mp*Rip1 which shares an overall 34% amino acid similarity with *Um*Rip1 was enough to recover its function as a ROS burst suppressor when expressed in planta. ROS burst assays with an unrelated mCherry protein fused to the RIFL motif, however, suggests that this motif alone is not sufficient for ROS burst suppression but works

712 only in the context of Rip1 like proteins. If the RIFL-motif is relevant for host protein
713 binding or necessary for the proper tertiary folding of Rip1 awaits future analysis.

714 The infection assays combining *rip1* deletion strains and *Zmlox3* mutant lines and the
715 respective combinations reveal that Rip1 in the context of the biotrophic interaction is
716 on its own a very good example for the iceberg model where recognition of effectors
717 and their activity keep each other usually in sum in a silent state(Thordal-Christensen,
718 2020). As Rip1 is widely conserved in smuts it can be assumed, that its virulence
719 promoting function supercedes its apparent costs which lead to reduced susceptibility
720 in the absence of Zmlox3. As Rip1 ROS-burst suppressive activities are demonstrated
721 in the monocot system maize as well as in the dicot *N. benthamiana* the targeted host-
722 pathways are highly conserved.

723 Zmlox3 itself is required for full susceptibility by many fungal pathogens in maize (Gao
724 et al., 2007). Assuming that due to co-evolution these pathogens might all cause
725 effector-triggered immune responses, employing a negative regulator of immunity as
726 a neutralizing measure would make sense. Considering the recently demonstrated
727 dependency of full ETI responses on functional PTI responses underlines the
728 relevance of PTI-suppressing effectors like Rip1 for pathogens (Yuan et al., 2021,
729 Ngou et al., 2021b).

730 In conclusion, we have established that Rip1 is a multifunctional core effector that
731 targets several conserved processes in different subcellular compartments in dicots
732 and monocots. This leads first of all to suppression of PTI responses. Beside this, we
733 find evidence that Rip1-dependent decrease of susceptibility of maize for *U. maydis* is
734 overcome by the presence of Zmlox3. Our data implicate, that Zmlox3 is a negative
735 regulator of immunity. We show, that the nuclear presence of Zmlox3, independent of
736 its known LOX activity is necessary for its ROS-burst suppressive function and that
737 Rip1 mediates ZmLox3 nuclear relocalisation by direct interaction. Future research will
738 be needed to focus on the enigmatic LOX-activity independent function of Zmlox3 and
739 its role in the plant nucleus in relation to plant immunity (Figure 6).

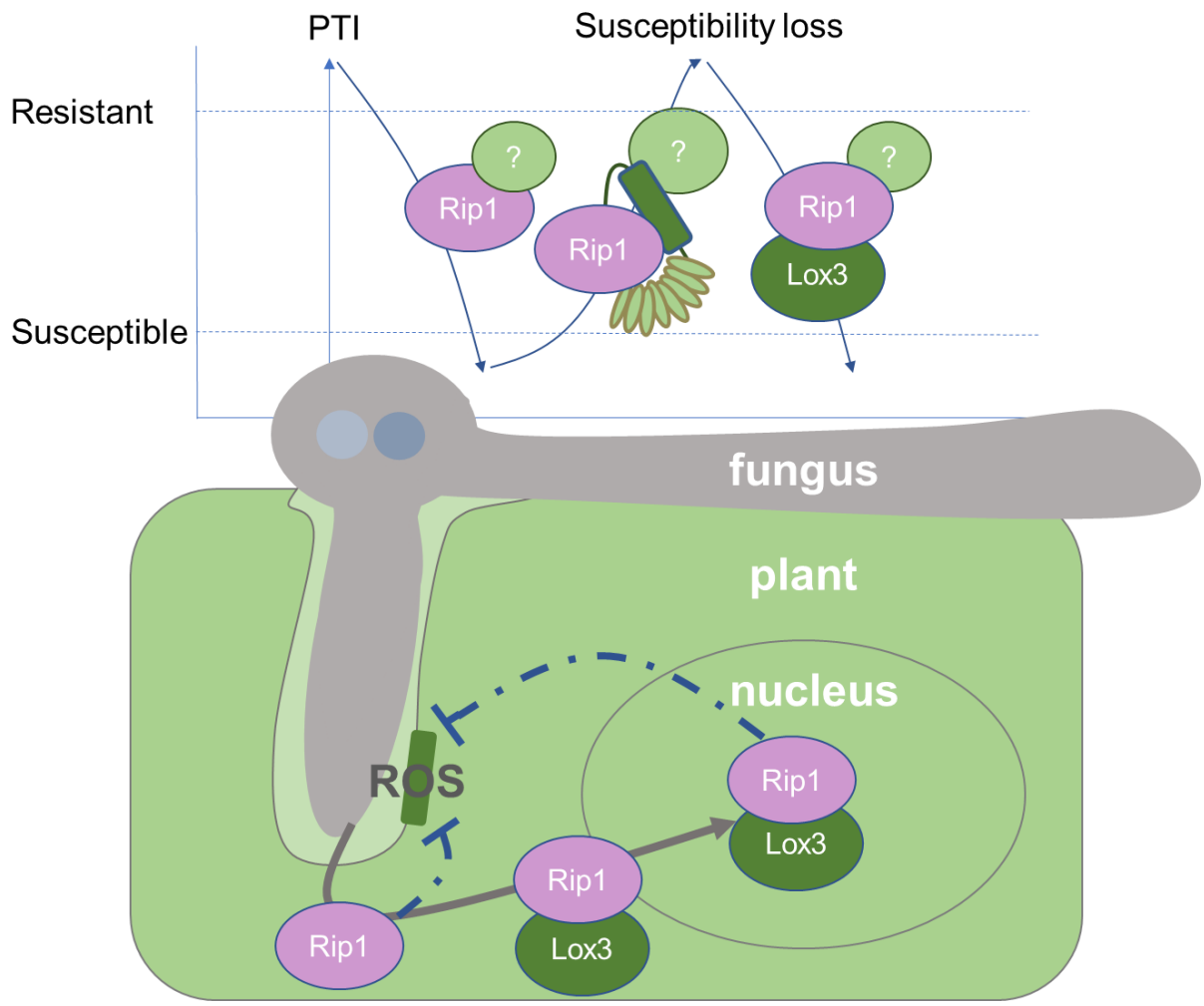

Figure 6*:* Model summarizing the role of Rip1 in the context of *U. maydis* maize interaction (left) and its specific interaction with Lox3 (right). (Rip1 = fungal effector, Lox3 = maize Lipoxygenase 3) left side: Rip1 suppresses PTI in the cytosol by a yet not identified mechanism. In the *U. maydis* /maize interaction, Rip1 is leading to Rip1-effector dependent loss of susceptibility of maize for *U. maydis,* but in presence of Lox3 compatibility is fully restored. Right: Rip1 is secreted by *U. maydis* and is translocated into the plant cell where it suppresses PTI responses. One of its targets is the maize lipoxygenase Lox3 which is shuttled by Rip1 into the nucleus where its lipoxygenase activity is not needed to contribute to ROS-burst suppression.

Material and Methods

Plasmids and cloning procedures

Escherichia coli Mach1 $T1^R$ (Thermo Fisher Scientific, Waltham, MS, USA) cells were used for cloning purposes. All plasmids were generated using standard molecular

cloning procedures (Sambrook et al., 1989) or by the GreenGate system (Lampropoulos et al., 2013). The modules used were either amplified by PCR or obtained by the aforementioned published system. Plasmids used for the purpose of the VIGS assay and the Y2H system, were based on the Gateway cloning system (Katzen, 2007). Point mutations were generated using QuikChange Mutagenesis. Restriction enzymes were purchased from New England Biolabs.

Generation of *U. maydis* strains and growth conditions

All *U. maydis* strains from this study are derived from the solopathogenic strain SG200 or AB33. For the deletion of *rip1*, strains were generated by gene replacement with a hygromycin cassette via homologous recombination with PCR-generated constructs(Bösch et al., 2016) or by insertions into the ip locus using p123 derivatives, as described previously (Loubradou et al., 2001). All generated constructs were sequenced prior to *U. maydis* transformation. For the complementation of Δ*rip1* mutants, linearized plasmids were integrated into the ip locus of SG200Δ*rip1*.

For induced filamentous growth assays, *U. maydis* strains were grown at 28°C with overnight shaking in YEPS light medium. The culture was next day set to OD_{600} = 1.0 in ddH_2O. The respective strains were spotted onto potato dextrose agar containing 1% activated charcoal after 2 days of growth.

All *U. maydis* strains were grown at 28°C in YEPSL (0.4% yeast extract, 0.4% peptone, 2% sucrose) and used for further experimental approaches.

Plant lines and plant growth conditions

Maize plants of the variety B73 and B73Δlox3 seeds were used for the experiments in this study.

N. benthamiana plants were grown in controlled short-day conditions (8h light/ 16h dark cycle; 22°C). *Zea mays* cv. B73 and B73Δ*lox3* (*lox3-4*) were grown in a temperature-controlled greenhouse (14h light/ 10h dark cycle; 28°C/20°C) and used for infection of *U. maydis*.

Maize and tassel infection assays

For disease scoring evaluation, *U. maydis* strains were grown in YEPSL (0.4% yeast extract, 0.4% peptone, 2% sucrose) and cell suspensions in H_2O were adjusted to an

optical density at λ600 nm of 1.0. into the stem of 7 days old maize seedlings of B73 or B73Δ*lox3*; cell suspensions were injected with a syringe as described (Kämper et al., 2006). Disease symptoms were scored 7 days post infection according to a previously developed scoring scheme (Kämper et al., 2006) and statistical analysis was performed as previously described (Stirnberg and Djamei, 2016).

Tassel infection were done in Gaspe Flint and symptoms of infected tassels were scored 14 days after the infection following the previous described scoring scheme (Redkar and Doehlemann, 2016).

Biolistic bombardment in *Z. mays*

For microscopy, 14 days old maize leaves were used for biolistic transformation. Plasmid DNA carrying the indicated gene under the CaMV35S promoter were coated with 1.6 µm gold particles and bombarded with the PDS-1000/He Particle Delivery System (Biorad) at 1100 p.s.i. Confocal microscopy was performed 2 days post transformation where fluorescence was observed. For ROS burst assays, 7 days old whole maize plants were bombarded with the appropriate FoMV construct encoding the respective gene and 8 to 9 days after, they were used for further analysis (Bouton et al., 2018).

Cell death assay in *N. benthamiana*

For selectively coloring of dead tissues, trypan blue staining was performed (Fernandez-Pozo et al., 2015). For this purpose, whole *N. benthamiana* leaves were used and completely immersed in a fresh prepared trypan blue solution (85% lactic acid, 99% glycerol, phenol, dd$H_2$0 and trypan blue). Stained leaves after 30 minutes were immediately washed with 98% ethanol a few times and then left in it overnight. Ethanol solution was then so often replaced till chlorophyll was completely washed out. Once colorless, ethanol was removed and replaced with 60% glycerol solution.Microscopy

Confocal microscopy was performed with Zeiss LSM 700 or LSM 780 confocal microscope. GFP was excited at 488 nm using an argon laser. Fluorescence emission was collected between 500-540 nm. mCherry was excited at 561 nm and emission was collected between 578-648 nm. Samples were placed on microscope slides, mounted in water and sealed with a cover slip. Images were post-processed and

analyzed using ZEN (black edition v2.3) and FIJI (https://imagej.net/Fiji) software packages. Images taken in red channels (mRFP, mCherry) were pseudo colored to magenta.

Fungal proliferation in infected maize tissue was observed using wheatgerm agglutinin (WGA) coupled to AlexaFluor488 (Invitrogen) which stains fungal hyphae. Propidium iodide (Sigma-Aldrich, St. Louis, MO, USA) was used to stain the plant cell wall. The area 1-3 cm below the infection point were excised and incubated into staining solution (1 µg/mL propidium iodide, 10 µg/mL WGA-AF488). Microscopy images were taken with Zeiss LSM780 confocal microscope. For WGA-AF488 the setting for excitation were at λ 488 nm and emission at λ 500–540 nm.

Protein secretion in axenic culture and *in planta*

U. maydis strain AB33 was used for protein secretion assays. Strain Potef::Rip1$_{1-166}$-HA was generated by insertion of plasmid p123-Potef::Rip1$_{1-166}$-HA into the *ip* locus of AB33 (Aichinger et al., 2003). Total protein fractions of *U. maydis* from cell pellets and culture supernatants were prepared as previously described by Djamei et al., 2011 (Djamei et al., 2011). Briefly, *U. maydis* cells were grown in CM medium with glucose. Proteins from supernatants were precipitated with trichloroacetic acid (TCA)/Sodium deoxycholate (DOC) and afterwards acetone-washed. Proteins from cell pellets and supernatant fractions were separated by SDS-PAGE and a Western blot was performed. Mouse monoclonal anti-hemagglutinin (HA; Vienna Biocenter Core Facilities) and mouse anti-actin (Sigma Aldrich, Calbiochem cat#CP01;lot#D00024369) antibodies were used for Western blot. Horseradish peroxidase-conjugated anti-mouse IgG (Cytiva, NXA931-1ML) was used as secondary antibody. Anti-Actin antibody was used as control for cell lysis as actin is not supposed to be secreted.

In planta the secretion was confirmed via confocal microscopy using generated strains SG200Δrip1-PCmu1::rip1$_{1-166}$-mCherry or SG200Δrip1-PCmu1::rip1$_{27-166}$-mCherry. Both strains were injected into 7 days-old maize seedlings and the mCherry signal was observed 5 days post infection.

Yeast transformation and yeast-two-hybrid interaction assays

For showing the interaction between Rip1$_{27-166}$ and Zmlox3 we used the yeast two hybrid assay Matchmaker™ GAL4 Two hybrid system (Clontech®, Mountain View,

CA, USA) following the manufacturer's protocol. The proteins tested for interaction were cloned into pGBKT7 or pGADT7 vectors, respectively. Here, we fused the yeast GAL4 binding (BD) to Zmlox3 and activation domain (AD) to Rip1 and transformed the constructs into the yeast strains Y187 (MAT α) or AH109 (MAT a), respectively. We selected yeast transformants after mating on selective dropout media (SD) lacking only tryptophan (Trp) and leucine (Leu). Protein interactions were assessed on SD selection medium lacking tryptophan, leucine, and histidine (His). Plates were incubated on 28°C and interaction was observed 4 days later.

Protein production in *N. benthamiana* and Co-immunoprecipitation

Four week-old *N. benthamiana* plants were co-infiltrated with *A. tumefaciens* carrying P35S::Rip1$_{27-166}$-mcherry-myc or P35S::mCherry-mcherry-myc and P35S::Zmlox3-GFP in a 1:1 ratio resuspended in ARM buffer (Agrobacterium resuspension medium, 10 mM MES-NaOH pH 5.6, 10 mM MgCl2, 150 µM Acetosyringone). Two leaves from each *N. benthamiana* plant were infiltrated and 48h later harvested and directly frozen in liquid nitrogen. Total proteins were extracted from 450 mg sample tissue and suspended in 2 ml IP buffer (HEPES 50 mM pH 7.5, NaCl 50 mM, Glycerol 10%, EDTA 1 mM, Triton X-100 0.05%, PMSF 1 mM and 1 protease inhibitor tablet; Roche). Extracts were cleared by centrifugation 10 min at 14000 x g; step was repeated at least 3 times. Protein pull-down was performed by adding 30 µl of anti-myc magnetic beads using the µMACS™ MicroBeads system from Miltenyi Biotech (Bergisch Gladbach, Germany) following the manuacturer's instructions. Briefly, samples were washed 4 times with 300 µl IP buffer and proteins were eluted by adding 120 µl of 2x SDS loading buffer at 95°C. 15-20 µl of the extracts were analyzed by SDS-PAGE followed by western blot with anti-myc (Santa Cruz Biotechnology, sc-789, lot#A1615) or anti-Zmlox3 (Kaneka Eurogentech S.A.) antibodies. As secondary antibody anti-rabbit IgG-HRP (Santa Cruz Biotechnology, sc-2357; lot#B0221) was used. Experiments were repeated at least 2 times.

Protein production and Lipoxygenase Activity Assay

For *in vivo* Lipoxygenase activity assays, ZmLox3 c-terminally fused to mCherry, mCherry-NLS or mCherry-NES and N-terminally tagged Zmlox3 with a 6xHis-tag were expressed in *E. coli* and affinity purified. Briefly, *E. coli* BL21 carrying the appropriate constructs were grown till OD_{600}=0.6 on 37°C. Afterwards, 1mM IPTG was added to

the cell cultures and were grow over night on 16°C. Cell cultures were harvested and total proteins were extracted in 20ml Extraction buffer (50mM Hepes, pH 8.0, 200mM NaCl, 1mM EDTA, 10% Glycerol , 20 mM Imidazole, 5mM beta-mercaptoethanol and 1mM PSMF). Samples were sonicated 5 times for 5 minutes with on-off modus to cool down the samples on ice. Cell debris was removed by ultracentrifugation at 4°C for 30 minutes at 15000rpm. The supernatant was then put into a 15ml Flacon tube and His-tag Ni NTA (Jena bioscience, AC-310-100) were applied and incubated for 1h shaking on 4°C. Then, supernatant was put into a column and let it to flow through. 10 resin volume of Wash buffer (50mM Hepes, pH 8.0, 200mM NaCl, 1mM EDTA, 10% Glycerol , 50 mM Imidazole, 5mM beta-mercaptoethanol and 1mM PSMF) were applied. Finally, the elution was carried out in a gradient with Elution buffer (50mM Hepes, pH 8.0, 200mM NaCl, 1mM EDTA, 10% Glycerol ,100mM, 200mM ,300mM, 400mM, 500mM Imidazole, 5mM beta-mercaptoethanol and 1mM PSMF) and run on a SDS-Page to visualize the proteins.

The Lipoxygenase activity assay was carried out as described by Xu et *al*., 2012 (Xu et al., 2012). Here, the substrates linoleic acid and linolenic acid were dissolved in absolute ethanol. Then around 2/3 of the prepared solution was supplemented with Tween 20. After removing the ethanol by rotary evaporator the residues were dissolved in 0.05 M Na_2HPO_4 and brought to a pH=9.0 with NaOH. Solutions were stored at 4°C in dark. The activity of ZmLox3 with Linolenic acid or Linoleic acid was measured in an absorbance at 234 nm on Thermo Scientific Spectronic Genesys 10 Bio UV-Visible Spectrophotometer. The reaction was initiated by adding into a thermally equilibrated cuvette, containing 100 µL of substrate solution and 1 mL of phosphate buffer, 25 µL of enzyme solution. The absorbance was recorded for 300 seconds. The experiment was repeated in two technical replicates.

Virus Induced Gene Silencing in *N. benthamiana*

Two-week old *N. benthamina* plants were infiltrated with *A. tumefaciens* GV3101 (pSoup). Cells were transformed carrying the appropriate construct pTRV1, pTRV2-Nblox6 and suspended in ARM buffer. Control plants were infiltrated with pTRV1 and either pTRV2-GFP. Cell suspensions were adjusted to an optical density at λ=600nm of 0.4. Suspensions of *A. tumefaciens* carrying pTRV1 and TRV2 with the respective construct were combined together at a ratio 1:1 and syringe infiltrated with a needle.

After two to three weeks, leaf discs were punched and analyzed. Experiments were repeated three times.

RNA extraction and Reverse transcriptase quantitative PCR

For expression levels of Nblox6 transcripts in VIGS plants, total RNA was isolated from three independent replicates of *N. benthamiana* leaves four to five weeks old. Complementary DNA (cDNA) was generated from total RNA using the iScript cDNA Synthesis Kit (BioRad). The FastStart Universal SYBR Green Master mix (Roche) was used to perform RT-qPCR experiments, according to manufacturer's protocol. The relative amount of amplicons in the samples were calculated with the $2^{-\Delta\Delta C}$ method (Livak & Schmittgen, 2001). Actin was used as reference gene (Nb AFD62804.1 (H9C954)).

Luminol-based ROS assays in *N. benthamiana* and *Z. mays*

N. benthamiana plants were grown for four to five weeks before *A. tumefaciens* infiltration with the appropriate construct, resuspended in MES buffer to a final optical density at 0.05 and 0.2. *Z. mays* plants were grown for seven days before biolistic bombardment was performed. Leaf discs of infiltrated *N. benthamiana* plants were punched 2 dpi and transformed maize surfaces indicated by mCherry fluorescence were punched 8 to 9 dpi and floated on water over night. Water was then exchanged with flg22 elicitation solution (10 µg/ml Peroxidase from Horseradish; Sigma Sigma-Aldrich cat# P6782, 34 µg/ml L-012; Fujifilm WAKO cat# 120-04891 and 100 nM flg22 in H_2O). Detection of ROS-burst in plant leaf discs was monitored by chemiluminescence over 45 minutes in a microplate reader (Tecan SparkR v 2.3 or Synergy H1, BioTek). All experiments were performed with three or five plants and at least repeated three times.

Pull-down assay and Mass Spectrometry

Nicotiana benthamiana leaves expressing $Rip1_{27\text{-}166}$-myc-mCherry were frozen in liquid nitrogen and grounded with mortar and pestle. Total proteins from $Rip1_{27\text{-}166}$-myc-mCherry and mcherry-myc-mCherry (used as control) were extracted as described(Kobayashi et al., 2015). Total protein extracts (4mg/IP) were immunopurified using anti-c-Myc antibody coupled very small magnetic beads

(MACS® Technology, Miltenyi) digested in column with trypsin, and analyzed in a single run on the mass spectrometer (Hubner et al., 2010).

The resulting tryptic peptide mixture was desalted prior LC-MS/MS analysis on a C18 ZipTip (Omix C18 100 ul tips, Varian), and the purified peptide mixture was analyzed by LC-MS/MS using a nanoflow RP-HPLC (LC program: linear gradient of 3-40 % B in 100 min, solvent A: 0.1% formic acid in water, solvent B: 0.1% formic acid in acetonitrile) on-line coupled to a linear ion trap-Orbitrap (Orbitrap-Fusion Lumos, Thermo Fisher Scientific) mass spectrometer operating in positive ion mode. Data acquisition was carried out in a data-dependent fashion, the 20 most abundant, multiply charged ions were selected from each MS survey for MS/MS analysis (MS spectra were acquired in the Orbitrap, and CID spectra in the linear ion trap).

Raw data were converted into peak lists using the in-house Proteome Discoverer (v 1.4) and searched against the Uniprot *Ustilago maydis* (USTMA) database (downloaded 2019.6.12, 6808 proteins) and the *Nicotiana benthamiana* protein database, 57140 proteins (Bombarely et al., 2012; Kourelis et al., 2019) using in-cloud Protein Prospector search engine (v5.15.1) with the following parameters: enzyme: trypsin with maximum 2 missed cleavage; mass accuracies: 5 ppm for precursor ions and 0.6 Da for fragment ions (both monoisotopic); fixed modification: carbamidomethylation of Cys residues; variable modifications: acetylation of protein N-termini; Met oxidation; cyclization of N-terminal Gln residues, allowing maximum 2 variable modifications per peptide. Acceptance criteria: minimum scores: 22 and 15; maximum E values: 0.01 and 0.05 for protein and peptide identifications, respectively. Spectral counting was used to estimate relative abundance of individual proteins in the no-antibody and c-Myc-mCherry negative controls and in the anti-c-Myc immuno purified samples (Jankovics et al., 2018).

Protein sequence analysis

Signal peptide prediction was performed with the program SignalP 5.0 (http://www.cbs.dtu.dk/services/SignalP/) (Almagro Armenteros et al., 2019). Sequence alignments were generated using Clustal Omega (http://www.ebi.ac.uk/Tools/msa/clustalo/) (Sievers et al., 2011). Secondary alpha helix structures were predicted with CLC Workbench 8.0. All images were processed using Inkscape (https://inkscape.org) and ImageJ (Schindelin et al., 2012).

Gene accession numbers

U. maydis (UMAG_04039) Gene Acc. Number: A0A0D1DWK7; *Sporisorium scitamineum* (SPSC_05323) Gene Acc. Number: CDS00260.1; *Ustilago hordei* (UHOR_13428) Gene Acc. Number: CCF48877.1; *Ustilago bromivora* (UBRO_13428) Gene Acc. Number: SAM84683.1 and *Melanopsichium pennsylvanicum* (BN887_05943) Gene Acc. Number: CDI54766.1; *N. benthamina* lipoxygenase 6 Gene Niben101Scf01434g03006.1; *Zea mays* lipoxygenase 3 Gene Acc. Number: NP_001105515.1.

Statistical analyses

Disease scoring in maize was evaluated using Fisher exact test, where the data was processed through a R-script previously described(Stirnberg and Djamei, 2016). Graphs and statistical analysis (the Student's t-test and Tukey's ANOVA) were performed using GraphPad Prism 8.0.

Acknowledgements

We thank the GMI (Vienna), the Plant Sciences Facility at Vienna BioCenter Core Facilities GmbH (VBCF) for support. Special thanks to Mr. Mathias Madalinski from the Protein Chemistry Core facility from VBC. We would also like to thank Dr. Krishna M. Pathi and Dr. Jochen Kumlehn from the Leibniz Institute of Plant Genetics and Crop Plant Research (IPK) for technical support. Additionally, we acknowledge Dr. Kostya Kanyuka from Rothamsted Research (UK) for kindly providing us the vector PV101 for virus-based protein expression in maize. We thank the Single Cell Omics Advanced Core Facility staff of the HCEMM and Biological Research Center for help with their resources and their support. We also thank Peter Baker, for the development and

maintenance of the ELKH Cloud (https://science-cloud.hu/) for hosting the ProteinProspector search engine.

The research leading to these results has received funding from the European Research Council under the European Union's Seventh Framework Programme ERC-2013-STG, Grant Agreement: 335691, the Austrian Science Fund (FWF): [I 3033-B22], the Austrian Academy of Sciences (OEAW) and the Deutsche Forschungsgemeinschaft (DFG, German Research Foundation) under Germany's Excellence Strategy (EXC 2070-390732324). A.P-S. was supported by the Development and Innovation Office of Hungary (GINOP-2.3.2-15-2016-00032).

Author Contribution

Conceptualization: Indira Saado, Armin Djamei

Funding acquisition: Armin Djamei

Contributions:

I.S., K.-S.C., R.B., A.A., F.N. conceived and performed experiments. F.N performed the initial identification of Rip1 as ROS Burst suppressive protein in plants. A.A. assisted with the TRV silencing and sample preparation for mass spectrometry experiments, K.-S.C. and R.B. assisted with microscopy experiments and data analysis. Mass spectrometry analysis was done by A.P.S.; LOX 3 mutant maize seeds were provided by M.V.K. and J.C.D. and I.F. helped with designing different LOX mutation versions and co-supervised experiments related to LOX activity. A.D. conceived the study and supervised the work. I.S. and A.D. wrote the manuscript with input from all co-authors.

Methodology: Indira Saado, Armin Djamei

Project administration: Indira Saado

Supervision: Armin Djamei

Writing: Indira Saado, Armin Djamei

Corresponding author

Correspondence to Armin Djamei.

Competing interests

The authors declare no competing interests.

REFERRENCES

Aichinger, C., Hansson, K., Eichhorn, H., Lessing, F., Mannhaupt, G., Mewes, W., Kahmann, R., 2003. Identification of plant-regulated genes in Ustilago maydis by enhancer-trapping mutagenesis. Mol. Genet. Genomics MGG 270, 303–314. https://doi.org/10.1007/s00438-003-0926-z

Ali, S., Laurie, J.D., Linning, R., Cervantes-Chávez, J.A., Gaudet, D., Bakkeren, G., 2014. An Immunity-Triggering Effector from the Barley Smut Fungus Ustilago hordei Resides in an Ustilaginaceae-Specific Cluster Bearing Signs of Transposable Element-Assisted Evolution. PLOS Pathog. 10, e1004223. https://doi.org/10.1371/journal.ppat.1004223

Almagro Armenteros, J.J., Tsirigos, K.D., Sønderby, C.K., Petersen, T.N., Winther, O., Brunak, S., von Heijne, G., Nielsen, H., 2019. SignalP 5.0 improves signal peptide predictions using deep neural networks. Nat. Biotechnol. 37, 420–423. https://doi.org/10.1038/s41587-019-0036-z

Bauer, R., Begerow, D., Oberwinkler, E., Piepenbring, M., Berbee, M.L., 2001. Ustilaginomycetes, in: McLaughlin, D.J., McLaughlin, E.G., Lemke, P.A. (Eds.), Systematics and Evolution, The Mycota. Springer, Berlin, Heidelberg, pp. 57–83. https://doi.org/10.1007/978-3-662-10189-6_3

Boller, T., Felix, G., 2009. A Renaissance of Elicitors: Perception of Microbe-Associated Molecular Patterns and Danger Signals by Pattern-Recognition Receptors. Annu. Rev. Plant Biol. 60, 379–406. https://doi.org/10.1146/annurev.arplant.57.032905.105346

Bombarely, A., Rosli, H.G., Vrebalov, J., Moffett, P., Mueller, L.A., Martin, G.B., 2012. A draft genome sequence of Nicotiana benthamiana to enhance molecular plant-microbe biology research. Mol. Plant-Microbe Interact. MPMI 25, 1523–1530. https://doi.org/10.1094/MPMI-06-12-0148-TA

Bösch, K., Frantzeskakis, L., Vraneš, M., Kämper, J., Schipper, K., Göhre, V., 2016. Genetic Manipulation of the Plant Pathogen Ustilago maydis to Study Fungal Biology and Plant Microbe Interactions. J. Vis. Exp. JoVE. https://doi.org/10.3791/54522

Bouton, C., King, R.C., Chen, H., Azhakanandam, K., Bieri, S., Hammond-Kosack, K.E., Kanyuka, K., 2018. Foxtail mosaic virus: A Viral Vector for Protein Expression in Cereals. Plant Physiol. 177, 1352–1367. https://doi.org/10.1104/pp.17.01679

Brachmann, A., Weinzierl, G., Kämper, J., Kahmann, R., 2001. Identification of genes in the bW/bE regulatory cascade in Ustilago maydis. Mol. Microbiol. 42, 1047–1063. https://doi.org/10.1046/j.1365-2958.2001.02699.x

Brock, T.G., Paine, R., Peters-Golden, M., 1994. Localization of 5-lipoxygenase to the nucleus of unstimulated rat basophilic leukemia cells. J. Biol. Chem. 269, 22059–22066.

Brockmann, B., Smith, M.W., Zaraisky, A.G., Harrison, K., Okada, K., Kamiya, Y., 2001. Subcellular localization and targeting of glucocorticoid receptor protein fusions expressed in transgenic Arabidopsis thaliana. Plant Cell Physiol. 42, 942–951. https://doi.org/10.1093/pcp/pce120

Cacas, J.-L., Vailleau, F., Davoine, C., Ennar, N., Agnel, J.-P., Tronchet, M., Ponchet, M., Blein, J.-P., Roby, D., Triantaphylides, C., Montillet, J.-L., 2005. The combined action of 9 lipoxygenase and galactolipase is sufficient to bring about programmed cell death during tobacco hypersensitive response. Plant Cell Environ. 28, 1367–1378. https://doi.org/10.1111/j.1365-3040.2005.01369.x

Chinchilla, D., Zipfel, C., Robatzek, S., Kemmerling, B., Nürnberger, T., Jones, J.D.G., Felix, G., Boller, T., 2007. A flagellin-induced complex of the receptor FLS2 and BAK1 initiates plant defence. Nature 448, 497–500. https://doi.org/10.1038/nature05999

Christensen, S.A., Kolomiets, M.V., 2011. The lipid language of plant–fungal interactions. Fungal Genet. Biol. 48, 4–14.

Christensen, S.A., Nemchenko, A., Park, Y.-S., Borrego, E., Huang, P.-C., Schmelz, E.A., Kunze, S., Feussner, I., Yalpani, N., Meeley, R., Kolomiets, M.V., 2014. The Novel Monocot-Specific 9-Lipoxygenase ZmLOX12 Is Required to Mount an Effective Jasmonate-Mediated Defense Against Fusarium verticillioides in Maize. Mol. Plant-Microbe Interactions® 27, 1263–1276. https://doi.org/10.1094/MPMI-06-13-0184-R

Constantino, N., Mastouri, F., Damarwinasis, R., Borrego, E., Moran-Diez, M.E., Kenerley, C.M., Gao, X., Kolomiets, M.V., 2013. Root-expressed maize lipoxygenase 3 negatively regulates induced systemic resistance to Colletotrichum graminicola in shoots. Front. Plant Sci. 4. https://doi.org/10.3389/fpls.2013.00510

Daguerre, Y., Plett, J.M., Veneault-Fourrey, C., 2016. Signaling pathways driving the development of ectomycorrhizal symbiosis, in: Molecular Mycorrhizal Symbiosis. John Wiley & Sons, Ltd, pp. 141–157. https://doi.org/10.1002/9781118951446.ch9

Darino, M., Chia, K.-S., Marques, J., Aleksza, D., Soto-Jiménez, L.M., Saado, I., Uhse, S., Borg, M., Betz, R., Bindics, J., Zienkiewicz, K., Feussner, I., Petit-Houdenot, Y., Djamei, A., 2021. Ustilago maydis effector Jsi1 interacts with Topless corepressor, hijacking plant jasmonate/ethylene signaling. New Phytol. 229, 3393–3407. https://doi.org/10.1111/nph.17116

Demchenko, K., Zdyb, A., Feussner, I., Pawlowski, K., 2012. Analysis of the subcellular localisation of lipoxygenase in legume and actinorhizal nodules. Plant Biol. 14, 56–63. https://doi.org/10.1111/j.1438-8677.2011.00480.x

Djamei, A., Schipper, K., Rabe, F., Ghosh, A., Vincon, V., Kahnt, J., Osorio, S., Tohge, T., Fernie, A.R., Feussner, I., Feussner, K., Meinicke, P., Stierhof, Y.-D., Schwarz, H., Macek, B., Mann, M., Kahmann, R., 2011. Metabolic priming by a secreted fungal effector. Nature 478, 395–398. https://doi.org/10.1038/nature10454

Doehlemann, G., Linde, K. van der, Aßmann, D., Schwammbach, D., Hof, A., Mohanty, A., Jackson, D., Kahmann, R., 2009. Pep1, a Secreted Effector Protein of Ustilago maydis, Is Required for Successful Invasion of Plant Cells. PLOS Pathog. 5, e1000290. https://doi.org/10.1371/journal.ppat.1000290

Doehlemann, G., Wahl, R., Horst, R.J., Voll, L.M., Usadel, B., Poree, F., Stitt, M., Pons-Kühnemann, J., Sonnewald, U., Kahmann, R., Kämper, J., 2008. Reprogramming a maize plant: transcriptional and metabolic changes induced by the fungal biotroph Ustilago maydis. Plant J. 56, 181–195. https://doi.org/10.1111/j.1365-313X.2008.03590.x

Dongus, J.A., Parker, J.E., 2021. EDS1 signalling: At the nexus of intracellular and surface receptor immunity. Curr. Opin. Plant Biol. 62, 102039. https://doi.org/10.1016/j.pbi.2021.102039

Estelle, D., Laurence, L., Marc, O., Caroline, D.C., Magali, D., Marie-Laure, F., 2020. Linolenic fatty acid hydroperoxide acts as biocide on plant pathogenic bacteria: Biophysical investigation of the mode of action. Bioorganic Chem. 100, 103877. https://doi.org/10.1016/j.bioorg.2020.103877

Fernández-Bautista, N., Domínguez-Núñez, J.A., Moreno, M.M.C., Berrocal-Lobo, M., 2016. Plant Tissue Trypan Blue Staining During Phytopathogen Infection. Bio-Protoc. 6, e2078–e2078.

Fernandez-Pozo, N., Rosli, H.G., Martin, G.B., Mueller, L.A., 2015. The SGN VIGS tool: user-friendly software to design virus-induced gene silencing (VIGS) constructs for functional genomics. Mol. Plant 8, 486–488. https://doi.org/10.1016/j.molp.2014.11.024

Feussner, I., Hause, B., Vörös, K., Parthier, B., Wasternack, C., 1995. Jasmonate-induced lipoxygenase forms are localized in chloroplasts of barley leaves (Hordeum vulgare cv. Salome). Plant J. 7, 949–957.

Flamand, N., Luo, M., Peters-Golden, M., Brock, T.G., 2009. Phosphorylation of serine 271 on 5-lipoxygenase and its role in nuclear export. J. Biol. Chem. 284, 306–313. https://doi.org/10.1074/jbc.M805593200

Foissner, I., Wendehenne, D., Langebartels, C., Durner, J., 2000. In vivo imaging of an elicitor-induced nitric oxide burst in tobacco. Plant J. 23, 817–824. https://doi.org/10.1046/j.1365-313X.2000.00835.x

Fukada, F., Rössel, N., Münch, K., Glatter, T., Kahmann, R., 2021. A small Ustilago maydis effector acts as a novel adhesin for hyphal aggregation in plant tumors. New Phytol. 231, 416–431. https://doi.org/10.1111/nph.17389

Gao, X., Brodhagen, M., Isakeit, T., Brown, S.H., Göbel, C., Betran, J., Feussner, I., Keller, N.P., Kolomiets, M.V., 2009. Inactivation of the lipoxygenase ZmLOX3 increases susceptibility of maize to Aspergillus spp. Mol. Plant-Microbe Interact. MPMI 22, 222–231. https://doi.org/10.1094/MPMI-22-2-0222

Gao, X., Shim, W.-B., Göbel, C., Kunze, S., Feussner, I., Meeley, R., Balint-Kurti, P., Kolomiets, M., 2007. Disruption of a maize 9-lipoxygenase results in increased resistance to fungal pathogens and reduced levels of contamination with mycotoxin fumonisin. Mol. Plant-Microbe Interact. MPMI 20, 922–933. https://doi.org/10.1094/MPMI-20-8-0922

Gaschler, M.M., Stockwell, B.R., 2017. Lipid peroxidation in cell death. Biochem. Biophys. Res. Commun. 482, 419–425. https://doi.org/10.1016/j.bbrc.2016.10.086

Genva, M., Obounou Akong, F., Andersson, M.X., Deleu, M., Lins, L., Fauconnier, M.-L., 2019. New insights into the biosynthesis of esterified oxylipins and their involvement in plant defense and developmental mechanisms. Phytochem. Rev. 18, 343–358. https://doi.org/10.1007/s11101-018-9595-8

Giraldo, M.C., Valent, B., 2013. Filamentous plant pathogen effectors in action. Nat. Rev. Microbiol. 11, 800–814. https://doi.org/10.1038/nrmicro3119

Hammarberg, T., Provost, P., Persson, B., Rådmark, O., 2000. The N-terminal Domain of 5-Lipoxygenase Binds Calcium and Mediates Calcium Stimulation of Enzyme Activity *. J. Biol. Chem. 275, 38787–38793. https://doi.org/10.1074/jbc.M006136200

He, Q., McLellan, H., Boevink, P.C., Birch, P.R.J., 2020. All Roads Lead to Susceptibility: The Many Modes of Action of Fungal and Oomycete Intracellular Effectors. Plant Commun., Special Issue on Plant-Pathogen Interactions (Organizing Editors: Paul Birch, Savithramma Dinesh-Kumar, Hui-Shan Guo, Ping He, Xin Li, Frank Takken, Yuanchao Wang) 1, 100050. https://doi.org/10.1016/j.xplc.2020.100050

Hemetsberger, C., Herrberger, C., Zechmann, B., Hillmer, M., Doehlemann, G., 2012. The Ustilago maydis Effector Pep1 Suppresses Plant Immunity by Inhibition of Host Peroxidase Activity. PLOS Pathog. 8, e1002684. https://doi.org/10.1371/journal.ppat.1002684

Hubner, N.C., Bird, A.W., Cox, J., Splettstoesser, B., Bandilla, P., Poser, I., Hyman, A., Mann, M., 2010. Quantitative proteomics combined with BAC TransgeneOmics reveals in vivo protein interactions. J. Cell Biol. 189, 739–754. https://doi.org/10.1083/jcb.200911091

Isakeit, T., Gao, X., Kolomiets, M., 2007. Increased Resistance of a Maize Mutant Lacking the 9-Lipoxygenase Gene, ZmLOX3, to Root Rot Caused by Exserohilum pedicellatum. J. Phytopathol. 155, 758–760. https://doi.org/10.1111/j.1439-0434.2007.01301.x

Jankovics, F., Bence, M., Sinka, R., Faragó, A., Bodai, L., Pettkó-Szandtner, A., Ibrahim, K., Takács, Z., Szarka-Kovács, A.B., Erdélyi, M., 2018. Drosophila small ovary gene is required for transposon silencing and heterochromatin organization, and ensures germline stem cell maintenance and differentiation. Dev. Camb. Engl. 145. https://doi.org/10.1242/dev.170639

Jeworutzki, E., Roelfsema, M.R.G., Anschütz, U., Krol, E., Elzenga, J.T.M., Felix, G., Boller, T., Hedrich, R., Becker, D., 2010. Early signaling through the Arabidopsis pattern recognition receptors FLS2 and EFR involves Ca-associated opening of plasma membrane anion channels. Plant J. Cell Mol. Biol. 62, 367–378. https://doi.org/10.1111/j.1365-313X.2010.04155.x

Jones, J.D.G., Dangl, J.L., 2006. The plant immune system. Nature 444, 323–329. https://doi.org/10.1038/nature05286

Jwa, N.-S., Hwang, B.K., 2017. Convergent Evolution of Pathogen Effectors toward Reactive Oxygen Species Signaling Networks in Plants. Front. Plant Sci. 8. https://doi.org/10.3389/fpls.2017.01687

Kämper, J., Kahmann, R., Bölker, M., Ma, L.-J., Brefort, T., Saville, B.J., Banuett, F., Kronstad, J.W., Gold, S.E., Müller, O., Perlin, M.H., Wösten, H.A.B., de Vries, R., Ruiz-Herrera, J., Reynaga-Peña, C.G., Snetselaar, K., McCann, M., Pérez-Martín, J., Feldbrügge, M., Basse, C.W., Steinberg, G., Ibeas, J.I., Holloman, W., Guzman, P., Farman, M., Stajich, J.E., Sentandreu, R., González-Prieto, J.M., Kennell, J.C., Molina, L., Schirawski, J., Mendoza-Mendoza, A., Greilinger, D., Münch, K., Rössel, N., Scherer, M., Vranes, M., Ladendorf, O., Vincon, V., Fuchs, U., Sandrock, B., Meng, S., Ho, E.C.H., Cahill, M.J., Boyce, K.J., Klose, J., Klosterman, S.J., Deelstra, H.J., Ortiz-Castellanos, L., Li, W., Sanchez-Alonso, P., Schreier, P.H., Häuser-Hahn, I., Vaupel, M., Koopmann, E., Friedrich, G., Voss, H., Schlüter, T., Margolis, J., Platt, D., Swimmer, C., Gnirke, A., Chen, F., Vysotskaia, V., Mannhaupt, G., Güldener, U., Münsterkötter, M., Haase, D., Oesterheld, M., Mewes, H.-W., Mauceli, E.W., DeCaprio, D., Wade, C.M., Butler, J., Young, S., Jaffe, D.B., Calvo, S., Nusbaum, C., Galagan, J., Birren, B.W., 2006. Insights from the genome of the biotrophic fungal plant pathogen Ustilago maydis. Nature 444, 97–101. https://doi.org/10.1038/nature05248

Katzen, F., 2007. Gateway(®) recombinational cloning: a biological operating system. Expert Opin. Drug Discov. 2, 571–589. https://doi.org/10.1517/17460441.2.4.571

Kim, J.H., Lee, S.-R., Li, L.-H., Park, H.-J., Park, J.-H., Lee, K.Y., Kim, M.-K., Shin, B.A., Choi, S.-Y., 2011. High cleavage efficiency of a 2A peptide derived from porcine teschovirus-1 in human cell lines, zebrafish and mice. PloS One 6, e18556. https://doi.org/10.1371/journal.pone.0018556

Kobayashi, K., Suzuki, Toshiya, Iwata, E., Nakamichi, N., Suzuki, Takamasa, Chen, P., Ohtani, M., Ishida, T., Hosoya, H., Müller, S., Leviczky, T., Pettkó-Szandtner, A., Darula, Z., Iwamoto, A., Nomoto, M., Tada, Y., Higashiyama, T., Demura, T., Doonan, J.H., Hauser, M.-T., Sugimoto, K., Umeda, M., Magyar, Z., Bögre, L., Ito, M., 2015. Transcriptional repression by MYB3R proteins regulates plant organ growth. EMBO J. 34, 1992–2007. https://doi.org/10.15252/embj.201490899

Kourelis, J., Kaschani, F., Grosse-Holz, F.M., Homma, F., Kaiser, M., van der Hoorn, R.A.L., 2019. A homology-guided, genome-based proteome for improved proteomics in the alloploid Nicotiana benthamiana. BMC Genomics 20, 722. https://doi.org/10.1186/s12864-019-6058-6

Lampropoulos, A., Sutikovic, Z., Wenzl, C., Maegele, I., Lohmann, J.U., Forner, J., 2013. GreenGate - A Novel, Versatile, and Efficient Cloning System for Plant Transgenesis. PLOS ONE 8, e83043. https://doi.org/10.1371/journal.pone.0083043

Lanver, D., Müller, A.N., Happel, P., Schweizer, G., Haas, F.B., Franitza, M., Pellegrin, C., Reissmann, S., Altmüller, J., Rensing, S.A., Kahmann, R., 2018. The Biotrophic Development of Ustilago maydis Studied by RNA-Seq Analysis. Plant Cell 30, 300–323. https://doi.org/10.1105/tpc.17.00764

Lapin, D., Bhandari, D.D., Parker, J.E., 2020. Origins and Immunity Networking Functions of EDS1 Family Proteins. Annu. Rev. Phytopathol. 58, 253–276. https://doi.org/10.1146/annurev-phyto-010820-012840

Lo Presti, L., Lanver, D., Schweizer, G., Tanaka, S., Liang, L., Tollot, M., Zuccaro, A., Reissmann, S., Kahmann, R., 2015. Fungal Effectors and Plant Susceptibility. Annu. Rev. Plant Biol. 66, 513–545. https://doi.org/10.1146/annurev-arplant-043014-114623

Loubradou, G., Brachmann, A., Feldbrügge, M., Kahmann, R., 2001. A homologue of the transcriptional repressor Ssn6p antagonizes cAMP signalling in Ustilago maydis. Mol. Microbiol. 40, 719–730. https://doi.org/10.1046/j.1365-2958.2001.02424.x

Luo, M., Jones, S.M., Peters-Golden, M., Brock, T.G., 2003. Nuclear localization of 5-lipoxygenase as a determinant of leukotriene B4 synthetic capacity. Proc. Natl. Acad. Sci. 100, 12165–12170. https://doi.org/10.1073/pnas.2133253100

Moore, J.W., Loake, G.J., Spoel, S.H., 2011. Transcription Dynamics in Plant Immunity. Plant Cell 23, 2809–2820. https://doi.org/10.1105/tpc.111.087346

Mueller, A.N., Ziemann, S., Treitschke, S., Aßmann, D., Doehlemann, G., 2013. Compatibility in the Ustilago maydis–Maize Interaction Requires Inhibition of Host Cysteine Proteases by the Fungal Effector Pit2. PLOS Pathog. 9, e1003177. https://doi.org/10.1371/journal.ppat.1003177

Navarrete, F., Gallei, M., Kornienko, A.E., Saado, I., Chia, K.-S., Darino, M.A., Khan, M., Bindics, J., Djamei, A., 2021a. TOPLESS promotes plant immunity by repressing auxin signaling and is targeted by the fungal effector Naked1. bioRxiv 2021.05.04.442566. https://doi.org/10.1101/2021.05.04.442566

Navarrete, F., Grujic, N., Stirnberg, A., Saado, I., Aleksza, D., Gallei, M., Adi, H., Alcântara, A., Khan, M., Bindics, J., Trujillo, M., Djamei, A., 2021b. The Pleiades are a cluster of fungal effectors that inhibit host defenses. PLOS Pathog. 17, e1009641. https://doi.org/10.1371/journal.ppat.1009641

Newcomer, M.E., Brash, A.R., 2015. The structural basis for specificity in lipoxygenase catalysis. Protein Sci. Publ. Protein Soc. 24, 298–309. https://doi.org/10.1002/pro.2626

Nomura, H., Komori, T., Uemura, S., Kanda, Y., Shimotani, K., Nakai, K., Furuichi, T., Takebayashi, K., Sugimoto, T., Sano, S., Suwastika, I.N., Fukusaki, E., Yoshioka, H., Nakahira, Y., Shiina, T., 2012. Chloroplast-mediated activation of plant immune signalling in Arabidopsis. Nat. Commun. 3, 926. https://doi.org/10.1038/ncomms1926

Nühse, T.S., Bottrill, A.R., Jones, A.M.E., Peck, S.C., 2007. Quantitative phosphoproteomic analysis of plasma membrane proteins reveals regulatory mechanisms of plant innate immune responses. Plant J. 51, 931–940. https://doi.org/10.1111/j.1365-313X.2007.03192.x

Okazaki, Y., Saito, K., 2014. Roles of lipids as signaling molecules and mitigators during stress response in plants. Plant J. 79, 584–596. https://doi.org/10.1111/tpj.12556

Pathi, K.M., Rink, P., Budhagatapalli, N., Betz, R., Saado, I., Hiekel, S., Becker, M., Djamei, A., Kumlehn, J., 2020. Engineering Smut Resistance in Maize by Site-Directed Mutagenesis of LIPOXYGENASE 3. Front. Plant Sci. 11. https://doi.org/10.3389/fpls.2020.543895

Raho, N., Ramirez, L., Lanteri, M.L., Gonorazky, G., Lamattina, L., ten Have, A., Laxalt, A.M., 2011. Phosphatidic acid production in chitosan-elicited tomato cells, via both phospholipase D and phospholipase C/diacylglycerol kinase, requires nitric oxide. J. Plant Physiol. 168, 534–539. https://doi.org/10.1016/j.jplph.2010.09.004

Ranf, S., Eschen-Lippold, L., Pecher, P., Lee, J., Scheel, D., 2011. Interplay between calcium signalling and early signalling elements during defence responses to microbe- or damage-associated molecular patterns. Plant J. Cell Mol. Biol. 68, 100–113. https://doi.org/10.1111/j.1365-313X.2011.04671.x

Redkar, A., Doehlemann, G., 2016. Ustilago maydis Virulence Assays in Maize. Bio-Protoc. 6, e1760–e1760.

Redkar, A., Hoser, R., Schilling, L., Zechmann, B., Krzymowska, M., Walbot, V., Doehlemann, G., 2015. A Secreted Effector Protein of Ustilago maydis Guides Maize Leaf Cells to Form Tumors. Plant Cell 27, 1332–1351. https://doi.org/10.1105/tpc.114.131086

Sambrook, J., Fritsch, E.F., Maniatis, T., 1989. Molecular cloning: a laboratory manual. Mol. Cloning Lab. Man.

Schindelin, J., Arganda-Carreras, I., Frise, E., Kaynig, V., Longair, M., Pietzsch, T., Preibisch, S., Rueden, C., Saalfeld, S., Schmid, B., Tinevez, J.-Y., White, D.J., Hartenstein, V., Eliceiri, K., Tomancak, P., Cardona, A., 2012. Fiji: an open-source platform for biological-image analysis. Nat. Methods 9, 676–682. https://doi.org/10.1038/nmeth.2019

Schuster, M., Schweizer, G., Kahmann, R., 2018. Comparative analyses of secreted proteins in plant pathogenic smut fungi and related basidiomycetes. Fungal Genet. Biol., Basidiomycete research in the post-genomic era 112, 21–30. https://doi.org/10.1016/j.fgb.2016.12.003

Sievers, F., Wilm, A., Dineen, D., Gibson, T.J., Karplus, K., Li, W., Lopez, R., McWilliam, H., Remmert, M., Söding, J., Thompson, J.D., Higgins, D.G., 2011. Fast, scalable generation of high-quality protein multiple sequence alignments using Clustal Omega. Mol. Syst. Biol. 7, 539. https://doi.org/10.1038/msb.2011.75

Smith, J., Heese, A., 2014. Rapid bioassay to measure early reactive oxygen species production in Arabidopsis leave tissue in response to living Pseudomonas syringae. Plant Methods 10, 6. https://doi.org/10.1186/1746-4811-10-6

Sohn, K.H., Segonzac, C., Rallapalli, G., Sarris, P.F., Woo, J.Y., Williams, S.J., Newman, T.E., Paek, K.H., Kobe, B., Jones, J.D.G., 2014. The nuclear immune receptor RPS4 is required for RRS1SLH1-dependent constitutive defense activation in Arabidopsis thaliana. PLoS Genet. 10, e1004655. https://doi.org/10.1371/journal.pgen.1004655

Stirnberg, A., Djamei, A., 2016. Characterization of ApB73, a virulence factor important for colonization of Zea mays by the smut Ustilago maydis. Mol. Plant Pathol. 17, 1467–1479. https://doi.org/10.1111/mpp.12442

Tanaka, S., Brefort, T., Neidig, N., Djamei, A., Kahnt, J., Vermerris, W., Koenig, S., Feussner, K., Feussner, I., Kahmann, R., 2014. A secreted Ustilago maydis effector promotes virulence by targeting anthocyanin biosynthesis in maize. eLife 3, e01355. https://doi.org/10.7554/eLife.01355

Thordal-Christensen, H., 2020. A holistic view on plant effector-triggered immunity presented as an iceberg model. Cell. Mol. Life Sci. https://doi.org/10.1007/s00018-020-03515-w

Tolley, J.P., Nagashima, Y., Gorman, Z., Kolomiets, M.V., Koiwa, H., 2018. Isoform-specific subcellular localization of Zea mays lipoxygenases and oxo-phytodienoate reductase 2. Plant Gene 13, 36–41. https://doi.org/10.1016/j.plgene.2017.12.002

Uhse, S., Djamei, A., 2018. Effectors of plant-colonizing fungi and beyond. PLoS Pathog. 14, e1006992. https://doi.org/10.1371/journal.ppat.1006992

Uhse, S., Pflug, F.G., Stirnberg, A., Ehrlinger, K., Haeseler, A. von, Djamei, A., 2018. In vivo insertion pool sequencing identifies virulence factors in a complex fungal–host interaction. PLOS Biol. 16, e2005129. https://doi.org/10.1371/journal.pbio.2005129

Vicente, J., Cascón, T., Vicedo, B., García-Agustín, P., Hamberg, M., Castresana, C., 2012. Role of 9-lipoxygenase and α-dioxygenase oxylipin pathways as modulators of local and systemic defense. Mol. Plant 5, 914–928. https://doi.org/10.1093/mp/ssr105

Wagner, S., Stuttmann, J., Rietz, S., Guerois, R., Brunstein, E., Bautor, J., Niefind, K., Parker, J.E., 2013. Structural basis for signaling by exclusive EDS1 heteromeric complexes with SAG101 or PAD4 in plant innate immunity. Cell Host Microbe 14, 619–630. https://doi.org/10.1016/j.chom.2013.11.006

Wang, K.-D., Borrego, E.J., Kenerley, C.M., Kolomiets, M.V., 2020. Oxylipins Other Than Jasmonic Acid Are Xylem-Resident Signals Regulating Systemic Resistance Induced by Trichoderma virens in Maize. Plant Cell 32, 166–185. https://doi.org/10.1105/tpc.19.00487

Wasternack, C., Feussner, I., 2018. The oxylipin pathways: biochemistry and function. Annu. Rev. Plant Biol. 69, 363–386.

Xu, B., Miao, W., Guo, K., Hu, Q., Li, B., Dong, Y., 2012. An improved method to characterize crude lipoxygenase extract from wheat germ. Qual. Assur. Saf. Crops Foods 4, 26–32. https://doi.org/10.1111/j.1757-837X.2011.00120.x

Yuan, M., Ngou, B.P.M., Ding, P., Xin, X.-F., 2021. PTI-ETI crosstalk: an integrative view of plant immunity. Curr. Opin. Plant Biol. 62, 102030. https://doi.org/10.1016/j.pbi.2021.102030

Zhou, J.-M., Zhang, Y., 2020. Plant Immunity: Danger Perception and Signaling. Cell 181, 978–989. https://doi.org/10.1016/j.cell.2020.04.028

NGOU, B. P. M., AHN, H. K., DING, P. & JONES, J. D. G. 2021b. Mutual potentiation of plant immunity by cell-surface and intracellular receptors. *Nature,* 592**,** 110-115.

YUAN, M., JIANG, Z., BI, G., NOMURA, K., LIU, M., WANG, Y., CAI, B., ZHOU, J. M., HE, S. Y. & XIN, X. F. 2021. Pattern-recognition receptors are required for NLR-mediated plant immunity. *Nature,* 592**,** 105-109.